RESEARCH ARTICLE

Open Access

IncRNA IGFL2-AS1 mediates NSCLC chemoresistance via YBX1-induced HSPA1A/RAP1 activation



Hongliang Dong^{1,2,3†}, Yunxiu Xia^{2,4†}, Jingjing Qi^{5†}, Cuilan Liu^{1,2,3}, Fei Wang^{1,2,3}, Bingjie Cui^{1,2,3}, Weiwei Chen^{1,2,3}, Wenwen Lv⁶, Nailiang Zhai¹, Jiong Deng^{1,2}, Yong Yu⁵, Fangling Ning³, Clemens A. Schmitt^{5,7,8,9,10*} and Jing Du^{1,2,3*}

[†]Hongliang Dong, Yunxiu Xia, and Jingjing Qi contributed equally to this work.

*Correspondence: clemens.schmitt@charite.de; diedith@bzmc.edu.cn

¹ Department of Respiratory and Critical Care Medicine, Binzhou Medical University Hospital, 661 Huanghe Second Road, 256600 Binzhou, People's Republic of China ⁵ Faculty of Medicine, Johannes Kepler University Linz, Altenberger Strasse 69, 4040 Linz, Austria Full list of author information is available at the end of the article

Abstract

Background: The development of drug resistance in cancer is associated with multiple malignant properties, including proliferative progression, metastasis, and stemness. Long noncoding RNAs (IncRNAs) reportedly contribute to multidrug resistance in lung cancer. However, functional and mechanistic studies of key IncRNAs associated with lung cancer are lacking.

Methods: Candidate IncRNA IGFL2-AS1 and its downstream target, the HSPA1A and RAP1 cascade, were identified using RNA sequencing. In vitro functional assays, including proliferation, clonal formation, Transwell migration, sphere formation, and drug sensitivity test, were conducted to explore the function of the IGFL2-AS1/HSPA1A axis in lung cancer. For in vivo functional validation, subcutaneous implantation and tail vein injection of luciferase-tagged lung cancer cells were performed in mouse models. Moreover, RNA pulldown, RNA immunoprecipitation (RIP), chromatin immunoprecipitation (ChIP), and point/truncated mutations were utilized to dissect the mechanisms underlying the activation of the YBX1-mediated IGFL2-AS1/HSPA1A axis. Pharmacological inhibition of HSPA1A was performed to restore chemotherapy sensitivity and attenuate lung cancer cell metastasis in vivo. Finally, tissue microarray staining was employed to evaluate the expression of the YBX1/IGFL2-AS1/HSPA1A/RAP1 axis in lung cancer specimens and its correlation with prognosis.

Results: IGFL2-AS1, stimulated by C/EBP β , was aberrantly upregulated in chemoresistant cell lines and lung cancer specimens. IGFL2-AS1 promoted lung cancer proliferation, metastasis, drug resistance, and stemness by upregulating HSPA1A expression both in vitro and in vivo. Mechanistically, IGFL2-AS1 recruited YBX1 to the HSPA1A promoter, facilitating its transcription. Pharmacological inhibition of HSPA1A restored the sensitization of A549 cells resistant to cisplatin and 5-fluorouracil via the downstream RAP1 signaling cascade. Notably, the YBX1/IGFL2-AS1/HSPA1A axis was consistently activated in lung cancer specimens and correlated with poor patient prognosis.

Conclusions: This study demonstrated that the YBX1-modulated IGFL2-AS1/HSPA1A/ RAP1 axis is aberrantly activated in lung cancer cells and is associated with unfavorable prognosis, highlighting its potential as a novel therapeutic target in clinical settings.



© The Author(s) 2025. **Open Access** This article is licensed under a Creative Commons Attribution-NonCommercial-NoDerivatives 4.0 International License, which permits any non-commercial use, sharing, distribution and reproduction in any medium or format, as long as you give appropriate credit to the original author(s) and the source, provide a link to the Creative Commons licence, and indicate if you modified the licensed material. You do not have permission under this licence to share adapted material derived from this article or parts of it. The images or other third party material in this article are included in the article's Creative Commons licence, unless indicated otherwise in a credit line to the material. If material is not included in the article's Creative Commons licence and your intended use is not permitted by statutory regulation or exceeds the permitted use, you will need to obtain permission directly from the copyright holder. To view a copy of this licence, visit http://creativecommons.org/licenses/by-nc-nd/4.0/.

Keywords: Lung cancer, Drug resistance, IGFL2-AS1, YBX1, HSPA1A

Introduction

Lung cancer is the leading cause of cancer mortality worldwide [1]. Pathologically, lung cancer is classified into two main subtypes: small cell lung cancer and non-small cell lung cancer (NSCLC), with the latter accounting for approximately 85% of all cases. Despite advancements in targeted and immunotherapies, cisplatin-based chemotherapy remains the first-line regimen for patients refractory to targeted therapy and immunotherapy. Moreover, only a limited subset of patients with lung cancer respond favorably. This is further complicated by the frequent development of resistance to conventional chemotherapy, which continues to hinder effective treatment outcomes in patients with lung cancer [2].

The development of drug resistance in cancer is orchestrated by a complex network of transcription factors (TFs) that bind to the enhancer or promoter regions of DNA sequences to regulate the transcription of target genes [3]. To date, approximately 1600 TFs have been identified in human cells, which collaborate with cofactors and mediators to maintain cellular homeostasis [4]. Well-studied oncogenic TFs, including nuclear factor (NF)-KB, signal transducer and activator of transcription 3 (STAT3), and hypoxia-inducible factor (HIF-1), promote the resistance of cancer cells to chemotherapy. In contrast, tumor-suppressing TFs, such as p53 and forkhead box O3 (FOXO3a), enhance cancer cell sensitivity to treatment [4]. CCAAT enhancer-binding proteins (C/ EBPs) form a family of six TFs with shared structural homology, exhibiting both tumorpromoting and tumor-suppressing functions [5]. C/EBPβ expression is significantly decreased in cervical cancer, with its overexpression inhibiting cellular proliferation and migration in vitro [6]. In triple-negative breast cancer, the inhibition of C/EΒPβ isoforms reduces cancer cell invasion by reversing the epithelial-mesenchymal transition (EMT) phenotype [7]. Additionally, the oncogenic TF, Y box binding protein 1 (YBX1), is upregulated in many cancer types and is associated with poor outcomes [8].

In addition to genetic mutations driving refractory cancer subgroups, RNA profiling has revealed that epigenetic remodeling, particularly the role of noncoding RNAs in directing oncogenic signaling, is instrumental in intrinsic and acquired drug resistance in cancer [9]. Long noncoding RNAs (lncRNAs), which are longer than 200 nucleotides, perform diverse physiological and pathological functions [10]. Recent studies have reported that lncRNAs may influence the effectiveness of multiple therapeutic strategies, including chemotherapy, radiotherapy, targeted therapy, and immune therapy, by regulating drug efflux, DNA damage repair, cell apoptosis, and oxidative stress [11, 12]. For instance, HOX transcript antisense RNA (HOTAIR), nicotinamide nucleotide transhydrogenase-antisense 1 (NNT-AS1), and linc00635 are upregulated in drug-resistant lung cancer cells and promote drug resistance. In contrast, lncRNA maternally expressed 3 (MEG3) is downregulated in cisplatin (DDP)-resistant cells and enhances the sensitivity of lung cancer cells to treatment by influencing p53 and BCL-xL (B-cell lymphomaextra-large) [13]. Additionally, RP11-350G8.5, a previously unexplored lncRNA, has emerged as a potential therapeutic target in patients with bortezomib-resistant multiple myeloma through a CRISPR-Cas9 screening strategy [14]. Notably, lncRNAs also play essential roles in influencing stemness features and the metastatic potential of cancer

cells [15–18]. Therefore, RNA-based therapies hold promising translational potential for various diseases, including viral infection and cancer [19], and identifying novel or potent lncRNA targets may inform the development of improved combination therapies for lung cancer.

Heat shock proteins (HSPs) are abnormally expressed in lung cancer specimens and are closely associated with cancer initiation, progression, and relapse [20]. Among HSPs, the role of the HSP70 family, encoded by HSPA genes, in tumorigenesis remains controversial. For instance, some members of the HSP70 family reportedly promote carcinogenesis and angiogenesis; however, HSP70 has also been reported to delay tumor progression by stimulating innate and adaptive immune responses [21, 22]. In particular, HSPA1A is activated upon proteasome inhibitor treatment in various malignant disorders, representing a vulnerability in drug-resistant cancer cells [23]. Moreover, HSPA1A is upregulated in glioblastoma multiforme tumors, promoting their proliferation and metastasis in vitro [24]. HSPA1A also enhances the immune activity of cytotoxic T lymphocytes in the tumor environment of colorectal cancer [25]. These data indicate that the pharmacological disruption of HSPA1A and its downstream signaling partners could represent a latent and potent strategy to facilitate lung cancer therapy. The present study aimed to identify novel lncRNA, which serves as a potential diagnostic marker or therapeutic target in lung cancer drug resistance and metastasis.

Methods

Cell culture and treatment

Human cell lines A549 (1101HUM-PUMC000002), H1299 (1101HUM-PUMC000469), H358 (1101HUM-PUMC000470), HEK-293T (1101HUM-PUMC00091), DDP-resistant cells (A549/DDP: 1101HUM-PUMC000519), and 5-FU-resistant cells (A549/5-FU: 1101HUM-PUMC000394) were purchased from Peking Union Medical College Cell Resource Center (Beijing, China). H520 (5301HUM-KCB13023YJ) was purchased from the Chinese Academy of Sciences Cell Bank (Kunming, China). SW900 (HTB-59) and HEBC (CRL-3245) were obtained from the American Type Culture Collection (Manassas, VA, USA). A549, H520, H1299, SW900, H358, A549/DDP, and A549/5-FU cells were cultivated in Roswell Park Memorial Institute (RPMI)-1640 medium supplemented with 10% fetal bovine serum (FBS; Hyclone, Utah, USA) and penicillin/streptomycin. HEBC and HEK-293T cells were cultured in Dulbecco's modified Eagle's medium (DMEM) supplemented with 10% FBS and penicillin/streptomycin. All cells were incubated at 37 °C in 5% CO₂. A549/DDP and A549/5-FU cells were cultured in RPMI-1640 medium supplemented with 10% FBS and DDP (2 μg/mL) or 5-FU (4 μg/mL).

Lentivirus and plasmid vector

IGFL2-AS1 overexpression and knockdown lentiviral vectors (pLent-EF1a-FH-CMV-copGFP-P2A-Puro-IGFL2-AS1-OE and pLent-U6-shRNA-CMV-copGFP-P2A-Puro-shRNA#2 or #3) were constructed by Shandong Weizhen Biotechnology Co., Ltd. Plasmid vectors (CEBP-β OE, YBX1 OE, YBX1#7, YBX1#8, YBX1#9, HSPA1A OE, HSPA1A#6, HSPA1A#7, and HSPA1A#8) were synthesized by Weizhen Biotechnology Co., Ltd. The remaining plasmid vectors (IGF2-AS1-Mut, YBX1-Flag, YBX1-Cut-Flag,

HSPA1A-Pro-WT, and HSPA1A-Pro-Mut) were synthesized by Shanghai GeneChem Co., Ltd.

Purification of cytoplasmic RNA and nuclear RNA

Cells (A549 and H520) were collected and lysed in lysis buffer J. After centrifugation, RNA was extracted from the supernatant and nucleus (cell pellet) using the Cytoplasmic and Nuclear RNA Purification Kit (AmyJet Scientific, Wuhan, China). RNA was reverse-transcribed to cDNA using the RevertAid First Strand cDNA Synthesis Kit (Thermo Fisher Scientific, Waltham, MA, USA). PCR was performed using 2×Taq PCR Mix (TIANGEN, Beijing, China) to detect the subcellular localization of *IGFL2-AS1*, normalized to the expression of *GAPDH* and *U6*.

Fluorescence in situ hybridization (FISH)

Labeled IGFL2-AS1 probes were synthesized by Boster Biological Technology; the probe sequence was as follows: IGFL2-AS1: 5′-Cy3 labeling-AGACCACATGGAGGA GACAGAGCCCTGATGTCCAGCTGA-3′. FISH was performed using a Fluorescent in Situ Hybridization Kit (Boster, Wuhan, China) according to the manufacturer's instructions. Images were obtained using a microscope (Olympus, Tokyo, Japan) at 200× magnification.

Luciferase reporter assay

To detect the binding sites of YBX1 on the *IGFL2-AS1* and *HSPA1A* promoters, fragments of the *IGFL2-AS1* and *HSPA1A* promoters or mutated fragments were cloned into the pGL3-basic vector (GeneChem, Shanghai, China) and transfected into HEK-293 T and H520 cells. Firefly luciferase activity was measured after 48 h using a Firefly and *Renilla* Dual Luciferase Assay Kit (UElandy, Suzhou, China), according to the manufacturer's instructions, with *Renilla* luciferase used as a transfection control.

Proliferative assay

Cells (3000 per well) were seeded in a 96-well plate. The proliferative capability of the cells was determined using the MCE Cell Counting Kit-8 (CCK8; MedChemExpress, Monmouth, NJ, USA), according to the manufacturer's instructions, after incubation for 0, 24, 48, 72, and 96 h. Absorbance was then measured at 450 and 630 nm using a microplate reader (Biotek, Synergy H1, Winooski, VT, USA). Relative proliferation was calculated as $(OD_{450} - OD_{630})_{Sample}/(OD_{450} - OD_{630})_{Control}$. For IC_{50} determination, cells (4000 per well) were seeded in a 96-well plate and treated with different concentrations of DDP and 5-FU (MedChemExpress). After 48 h, CCK8 mixed with RPMI-1640 was used for the cell viability assay, and absorbance was measured at 450 and 630 nm.

Colony formation assay

Cells (600 cells per well) were seeded in six-well plates. After 2 weeks, the cells were fixed with 4% paraformaldehyde (Sangon Biotech, Shanghai, China) for 15 min and stained with Crystal Violet (Sangon Biotech) for an additional 15 min. Images were obtained using a microscope (Olympus, Japan) and analyzed using ImageJ software (National Institutes of Health, Bethesda, MD, USA).

Wound healing assay

Cells $(1\times10^5~\text{cells/well})$ were seeded into 12-well plates and incubated for 24 h. A scratch was created using a 200 μL tip of a pipette tip and washed with phosphate-buffered saline (PBS). Cells were incubated in a serum-free medium for 48 h; photomicrographs were taken with an IX53 inverted microscope and DP73 color camera (Olympus). The distance relative to the remaining wound area was calculated.

Transwell assay

Cells were suspended in 200 μ L of RPMI-1640 medium (Biological Industries, Beit Haemek, Israel) without FBS and seeded in the top chamber of Transwell inserts (Corning Inc., Corning, NY, USA). The lower chambers contained 800 μ L of RPMI-1640 medium with 20% FBS. After 72 h, the upper compartment cells were removed using a swab, and the chamber was washed with PBS, stained with crystal violet for 1 min, and washed again with PBS. The plates were imaged using an IX53 inverted fluorescence microscope and a DP73 color camera (Olympus, Japan). Image J was used to screen and analyze the densitometry of each visual field.

Sphere formation assay

Cells (2000 per well) were seeded into 12-well plates in serum-free RPMI-1640 medium (1 mL), containing 20 ng/mL fibroblast growth factor Peprotech, Cranbury, NJ, USA), 20 ng/mL epidermal growth factor (Peprotech), and 2% B27 (Thermo Fisher Scientific). RPMI-1640 medium (500 μ L) was added every 5 days. After 10 days, the spheroids were photographed and counted using an IX53 inverted fluorescence microscope and a DP73 color camera (Olympus).

Apoptosis assay

Cells (1×10°) were collected and processed with the fluorescein isothiocyanate (FITC)-Annexin V/propidium iodide (PI) Apoptosis Detection Kit (Uelandy, Suzhou, China) according to the manufacturer's instructions. Cellular apoptosis was then analyzed using flow cytometry (CytoFLEX SRT; Beckman Coulter, Brea, CA, USA).

Quantitative real-time PCR (qRT-PCR) analysis

Total RNA was extracted from tumors or cells using TRIzol reagent (Thermo Fisher Scientific) and reverse-transcribed to cDNA using the RevertAid First Strand cDNA Synthesis Kit (Thermo Fisher Scientific). qRT-PCR was performed using $2\times EasyTaq^{\$}$ PCR SuperMix (TransGen Biotech, Beijing, China). The relative expression level of the mRNA of genes was determined using the $2^{-\Delta\Delta CT}$ method and normalized to *GAPDH*. All primers are listed in Additional File 1: Table 1.

Western blot

Cells were collected and lysed with RIPA lysis buffer (Solarbio, Beijing, China) containing phenylmethanesulfonyl fluoride (Solarbio) on ice for 30 min. The supernatant was harvested after centrifugation (16,000g, 10 min), and the protein concentration was measured using a bicinchoninic acid (BCA) protein assay kit (Sangon Biotech). Protein (30 μ g/sample) was separated on sodium dodecyl sulfate (SDS)-polyacrylamide gel

electrophoresis (PAGE) gels and transferred to polyvinylidene fluoride membranes using electroblotting. Membranes were blocked with 5% milk at 25 °C for 1 h and then incubated at 4 °C for 12 h with primary antibodies. They were incubated with the secondary antibody for 2 h at 37 °C. Finally, the immunoreaction was visualized using enhanced chemiluminescence (ECL) horseradish peroxidase (HRP) substrates and detected using Bio-Rad ChemiDoc XRS (Bio-Rad Laboratories, Hercules, CA, USA). The band intensity was quantified using ImageJ software (National Institutes of Health, Bethesda, Maryland, USA). All antibodies are listed in Additional File 1: Table 2.

RNA immunoprecipitation (RIP) assay

The RIP assay was performed with the Magna RIP^{TM} RNA-Binding Protein Immunoprecipitation Kit (MilliporeSigma, Burlington, MA, USA) according to the manufacturer's instructions. Briefly, cells (1×10^8) were collected and chilled in polysome lysis buffer for 15 min on ice. The cell lysates were incubated with RIP buffer containing magnetic beads conjugated with the indicated antibodies or immunoglobulin G (IgG). After vortexing overnight at 4 °C, the mixtures were digested with proteinase K (MedChemExpress) at 55 °C for 30 min. The supernatant was harvested, RNA was extracted, and target genes were detected using qRT-PCR.

Chromatin immunoprecipitation (ChIP)

ChIP was performed with the Magna ChIP® HiSens Chromatin Immunoprecipitation Kit (MilliporeSigma) according to the manufacturer's instructions. Cells (2×10^8) were fixed with 37% formaldehyde and quenched with 2.5 M glycine, washed with ice-cold PBS, and lysed in a buffer containing protease inhibitors. Chromatin DNA was fragmented into 100-500-bp segments via sonication. Lysates containing DNA fragments were incubated with 5 μ g of the corresponding antibody and control IgG antibody at 4 °C overnight. Chromatin–antibody complexes were precipitated with magnetic beads and washed with lysis buffer and $1\times$ Tris-buffered saline (TBS). The crosslinks were reversed through incubation at 65 °C overnight. Eluted DNA was collected using Dzup Genomic DNA Isolation Reagent (Sangon Biotech) and analyzed by PCR. The primers are listed in Additional File 1: Table 3.

RNA pulldown and mass spectrometry (MS) analysis

RNA probes were labeled with biotin using a T7 Transcription Kit (RiboBio, Guangzhou, China), and RNA pulldown assays were performed using the BersinBio[™] RNA Pulldown Kit (BersinBio, Guangzhou, China) according to the manufacturer's instructions. Protein samples were loaded onto each lane of an SDS-PAGE gel, electrophoresed, and stained with Coomassie Brilliant Blue (Sangon Biotech). The target regions were excised and subjected to MS analysis (Novogene, Beijing, China). The primers are listed in Additional File 1: Table 1.

RNA sequencing and data analysis

Total RNA was extracted using TRIzol reagent (Thermo Fisher Scientific). lncRNA sequencing was performed by BGI (Shenzhen, China). RNA sequencing was performed using the Novogene software. The raw FASTQ file was cleaned of adapters using

Trimomatic (version 0.39). To map the sequencing reads to the human reference genome (GRCh28.p13), the HISAT2 (2.2.1) alignment tool was used. Gene expression was quantified using the featureCounts (v2.0.1) tool, which assigns sequencing reads to individual genes (Gencode. v38.annotatios), providing raw gene expression data for downstream analysis.

Differential gene expression analysis

Differential gene expression analysis was performed using the edgeR (3.42.4) R package. A standard DESeq2 workflow was performed on the basis of the mean of normalized counts to optimize detection power while controlling for false discovery rate. Differentially expressed genes (DEGs) were identified using edgeR, defined by $|\log_2 FC| \ge 1$ (\ge twofold change) and FDR < 0.05 (Benjamini–Hochberg correction). Pathway analysis was conducted using the R package ClusterProfiler (version 4.8.3).

Immunohistochemical (IHC) staining

Paraffin-embedded slices (4 μ m) were dried at 60 °C for 1 h and dewaxed twice with fresh xylene, followed by hydration using an alcohol gradient. After blocking endogenous peroxidase with 3% H_2O_2 , the samples were immersed in an antigen retrieval buffer at 100 °C for 5 min and cooled to 20–25 °C. Primary antibodies were incubated with the samples at 4 °C overnight, followed by incubation with secondary antibodies at room temperature for 1 h. Proteins were visualized using 3,3′-diaminobenzidine (DAB) chromogenic substrate (Boster, Wuhan, China) and counterstained with hematoxylin (Boster). Images were captured using a microscope (Olympus) at 200× magnification. The antibodies are listed in Additional File 1: Table 2.

In vivo tumor growth assay and lung metastasis model

All animal experiments were carried out according to the Health Guide for the Care and Use of Laboratory Animals and approved by the Animal Experimental Research Ethics Committee of Binzhou Medical University Hospital (approval no. 20221014-101).

Six- to eight-week-old female BALB/c nude mice were obtained from Ji'nan Pengyue Laboratory Animal Breeding Co., Ltd. (Ji'nan, China). To generate the tumor xenograft model, luciferase-labeled cells (5×10^6) were injected subcutaneously into the armpits of nude mice. Two weeks after the injection, saline or drugs were administered (Fig. 3A and Fig. 8A). The fluorescence intensity of the tumor tissues at different time points was detected using the CRI Maestro noninvasive fluorescence imaging system. All mice were euthanized by excess CO_2 , and the tumors were excised and weighed at the end of the treatment. Tumor volume was calculated using the following formula: $V = (length \times width^2)/2$.

For the lung metastasis model, 5×10^6 luciferase-labeled cells were injected into the tail veins. All mice were monitored using the CRI Maestro noninvasive fluorescence imaging system (Fig. 3G). Saline or other drugs were administered from weeks 1 to 6 (Fig. 8A). Lung metastasis was detected at weeks 1, 3, and 6. After 8 weeks, all mice were euthanized, and the lungs were excised for pathological examination, hematoxylin and eosin (H&E) staining, and lung metastatic nodule enumeration.

Microarray and data analysis

A tissue microarray (HLugA180Su11, Additional File 1: Table 4) was obtained, and in situ hybridization (ISH) of lncRNA and IHC was performed by Shanghai Outdo Biotech Co., Ltd. (Shanghai, China) to detect the transcription levels of *IGFL2-AS1* and the expression levels of YBX1 and HSPA1A. The results were screened and scored according to the signal intensity. Staining was classified as weakly, moderately, or strongly positive and appeared light yellow (1+), brownish yellow (2+), or brown (3+), respectively.

Genomic predictive analysis

The predicted *IGFL2-AS1* transcriptional regulators were identified using the PROMO and GeneCards databases. The potential coding capacity of IGFL2-AS1 was evaluated using the LNCipedia database. The predicted secondary structure of IGFL2-AS1 was determined using RNAalifold (http://rna.tbi.univie.ac.at/cgi-bin/RNAWebSuite/RNAfold.cgi). The predicted binding regions between IGFL2-AS1 and YBX1 were identified using catRAPID omics v2.1 (http://s.tartaglialab.com/page/catrapid_group). The YBX1 binding sites on IGFL2-AS1 and HSPA1A were predicted using JASPAR (http://jaspar.genereg.net/).

Statistical analysis

Statistical analyses were performed using Prism software (version 8.0; GraphPad Inc., San Diego, CA, USA). Patients were stratified into high-expression and low-expression groups based on the median H-score of genes. Overall survival (OS) was evaluated using the Kaplan–Meier survival analysis and examined using the log-rank (Mantel–Cox) test. Correlation analysis was performed using Spearman's correlation coefficient. Data are presented as mean \pm standard deviation. Each experiment was repeated at least three times, with at least three replicates per group. Comparisons between two groups were performed using two-tailed Student's t-tests. Multiple comparisons were performed using one-way or two-way analysis of variance (ANOVA). P-value < 0.05 was considered significant.

Results

IGFL2-AS1 is upregulated in drug-resistant lung cancer cells and predicts poor survival in patients with lung cancer

To mimic drug resistance developed during clinical treatment, commercially available DDP-resistant A549 cells, established through long-term drug exposure, were used as a secondary resistance model (SR). A549 cells that survived continuous treatment for 10 days served as the primary resistance model (PR). Parental A549 cells (PC) were used as controls for high-throughput RNA sequencing. The resistance index of SR to PC, which had been previously reported, was validated using the CCK8 assay (Additional File 3: Fig. S1A) [17].

Kyoto Encyclopedia of Genes and Genomes (KEGG) analysis revealed enrichment of multiple oncogenic signaling cascades, including RAP1, Hippo, mammalian target of rapamycin (mTOR), FOXO, AMP-activated protein kinase (AMPK), and

Hedgehog, in chemo-drug-resistant cells, which confirmed the carcinogenic nature of the DDP-resistant model (Additional File 3: Fig. S1B). Based on a $-\log_{10}$ -adjusted P-value threshold set at 20, a total of 17 and 6 lncRNAs were identified to be significantly dysregulated in SR and PR cells, respectively, compared with PC A549 cells. Notably, IGFL2-AS1 was among the top upregulated lncRNAs in both SR and PR lung cancer cells compared with parental lung cancer cells; thus, it was selected for further validation and investigation (Fig. 1A, B). The upregulation of IGFL2-AS1 was first verified in DDP-resistant and 5-fluorouracil (5-FU)-resistant A549 cells compared with parental cells (Fig. 1C). IGFL2-AS1 expression was quantified in immortalized human bronchial epithelial cells (HBECs), lung adenocarcinoma cells (A549, H1299, and H358), and lung squamous carcinoma cells (H520 and SW900), revealing its aberrantly upregulation in all lung cancer cells compared with HBECs (Fig. 1D). For further gain- and loss-of-function analyses, A549 and H520 cells, representing lung adenocarcinoma (LUAD) and lung squamous carcinoma, respectively, were used for functional and mechanistic studies.

FISH staining revealed that IGFL2-AS1 was primarily located in the nuclei of A549 and H520 cells (Fig. 1E). qRT-PCR amplification upon nucleoplasmic separation confirmed that IGFL2-AS1 was located mainly in the nucleus of lung cancer cells, compared with U6 and GAPDH, which are markers of the nucleus and cytoplasm, respectively (Fig. 1F). Immunohistochemical staining of the tissue microarray demonstrated that IGFL2-AS1 was markedly upregulated in lung cancer tissues compared with paired para-carcinoma tissues (Fig. 1G). Kaplan–Meier curve analysis, performed using a tissue microarray cohort, indicated that high IGFL2-AS1 expression was negatively correlated with the overall survival (OS) rate of patients with lung cancer, suggesting its oncogenic role (Fig. 1H); detailed information is presented in Additional File 1: Table 4. Moreover, LNCipedia analysis predicted that *IGFL2-AS1* had no protein-coding potential, suggesting that it functions as a traditional lncRNA (Additional File 3: Fig. S1C).

IGFL2-AS1 modulates lung cancer cell proliferation, metastasis, stemness, and multidrug resistance in vitro

Gain-of-function and loss-of-function analyses were performed in vitro using A549 and H520 cells to evaluate the effect of IGFL2-AS1 on lung cancer. The upregulation efficacy of the exogenous IGFL2-AS1 plasmid was verified using qRT-PCR (Fig. 2A). Overexpression of IGFL2-AS1 markedly increased the proliferative capacity (Fig. 2B, C) and migration of lung cancer cells (Fig. 2D; Additional File 4: Fig. S2A). In cells with IGFL2-AS1 overexpression, the EMT-related markers Snail, Twist, and vimentin were upregulated, whereas E-cadherin expression was downregulated (Additional File 4: Fig. S2B). In A549 and H520 lung cancer cells, exogenous IGFL2-AS1 overexpression promoted the proliferation of stem-like cells and upregulated the expression of stem cell-specific markers, namely, ATP-binding cassette superfamily G member 2 (ABCG2), octamer-binding transcription factor 4 (OCT4), and Nanog homeobox (NANOG) (Fig. 2E; Additional File 4: Fig. S2C). CCK8 assays further demonstrated that IGFL2-AS1 overexpression significantly increased the IC_{50} values of DDP and 5-FU but not of gefitinib and osimertinib (data not shown) in A549 and H520 cells (Fig. 2F). These results suggest that IGFL2-AS1 expression is positively related to chemo-drug resistance in lung cancer cells.

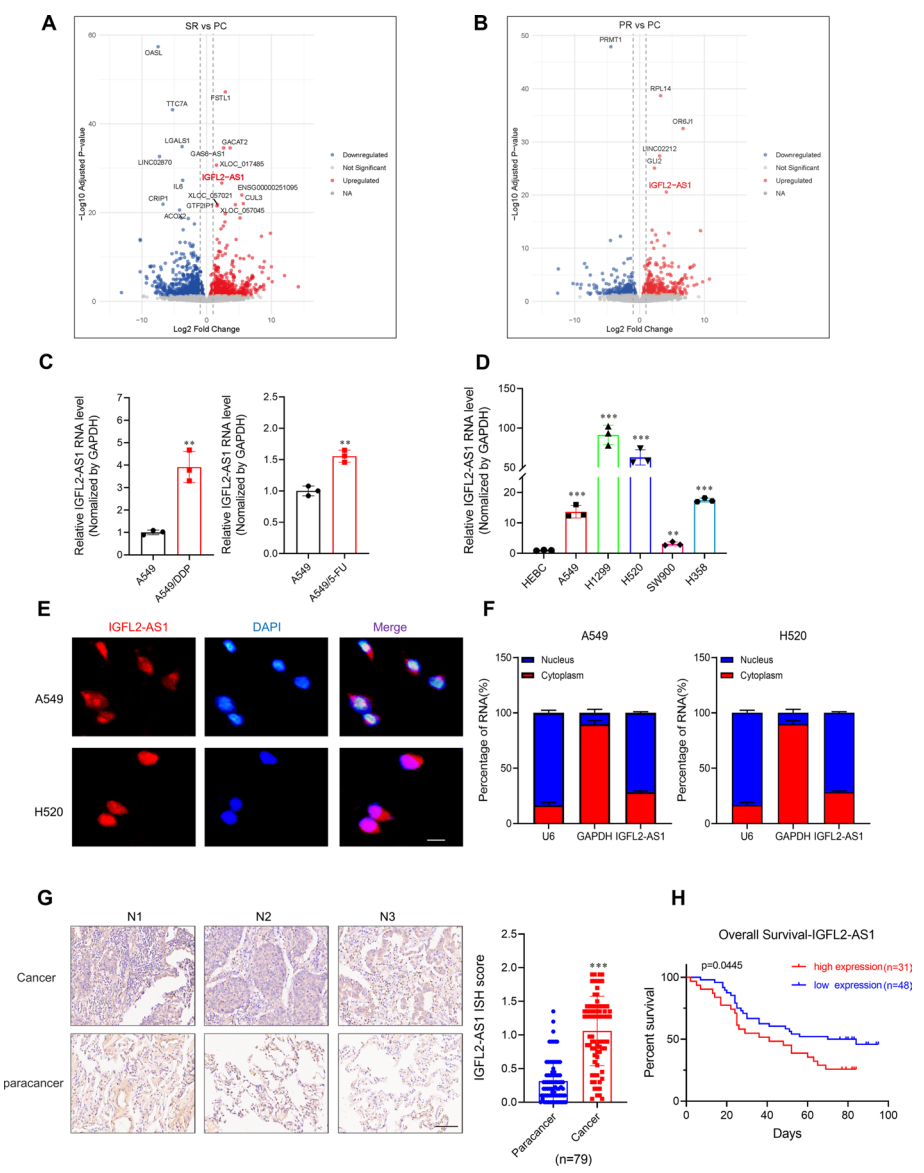


Fig. 1 IGFL2-AS1 is aberrantly upregulated in drug-resistant lung cancer cells and predicts poor survival in patients. A Volcano plot of IncRNAs upregulated and downregulated in DDP secondary resistant cells (SR) compared with parental A549 cells (PC) based on IncRNA high-throughput sequencing. **B** Volcano plot of IncRNAs upregulated and downregulated in DDP primary resistant cells (PR) compared with parental A549 cells (PC) based on IncRNA high-throughput sequencing. IGFL2-AS1 is highlighted as a top candidate. C Upregulation of IGFL2-AS1 in DDP- (left) or 5-FU-resistant (right) A549 cells compared with parental cells, as detected via qRT-PCR. D Transcription level of IGFL2-AS1 in HEBC and lung cancer cells measured using qRT-PCR. E FISH staining of IGFL2-AS1 in A549 and H520 cells. As a counterstain for nuclei, 4',6-diamidino-2-phenylindole (DAPI) was used. Scale bar, 10 μ m. **F** Cellular distribution of IGFL2-AS1 transcripts in A549 and H520 cells detected via RNA fractionation combined with qRT-PCR. U6 (nuclear) and GAPDH (cytoplasmic) are positive controls. G Representative images (left) and quantification (right) of IGFL2-AS1 expression in paired cancer and adjacent normal lung tissues (n = 79 pairs), as detected using RNA in situ hybridization of tissue microarrays. Scale bar, 200 μ m. **H** Kaplan–Meier curve of the overall survival of patients with lung cancer (total n = 79) based on IGFL2-AS1 expression. The red line represents the high-expression group (n = 31, H-score > 1.275), while the blue line denotes the low-expression group (n = 48, H-score ≤ 1.275). All plots are presented as the mean ± SD. Statistical analyses: two-tailed unpaired Student's t-test (**C** and **D**), two-tailed paired Student's t-test (**G**), log-rank (Mantel–Cox) test (**H**). *P< 0.05, **P< 0.01, ***P<0.001

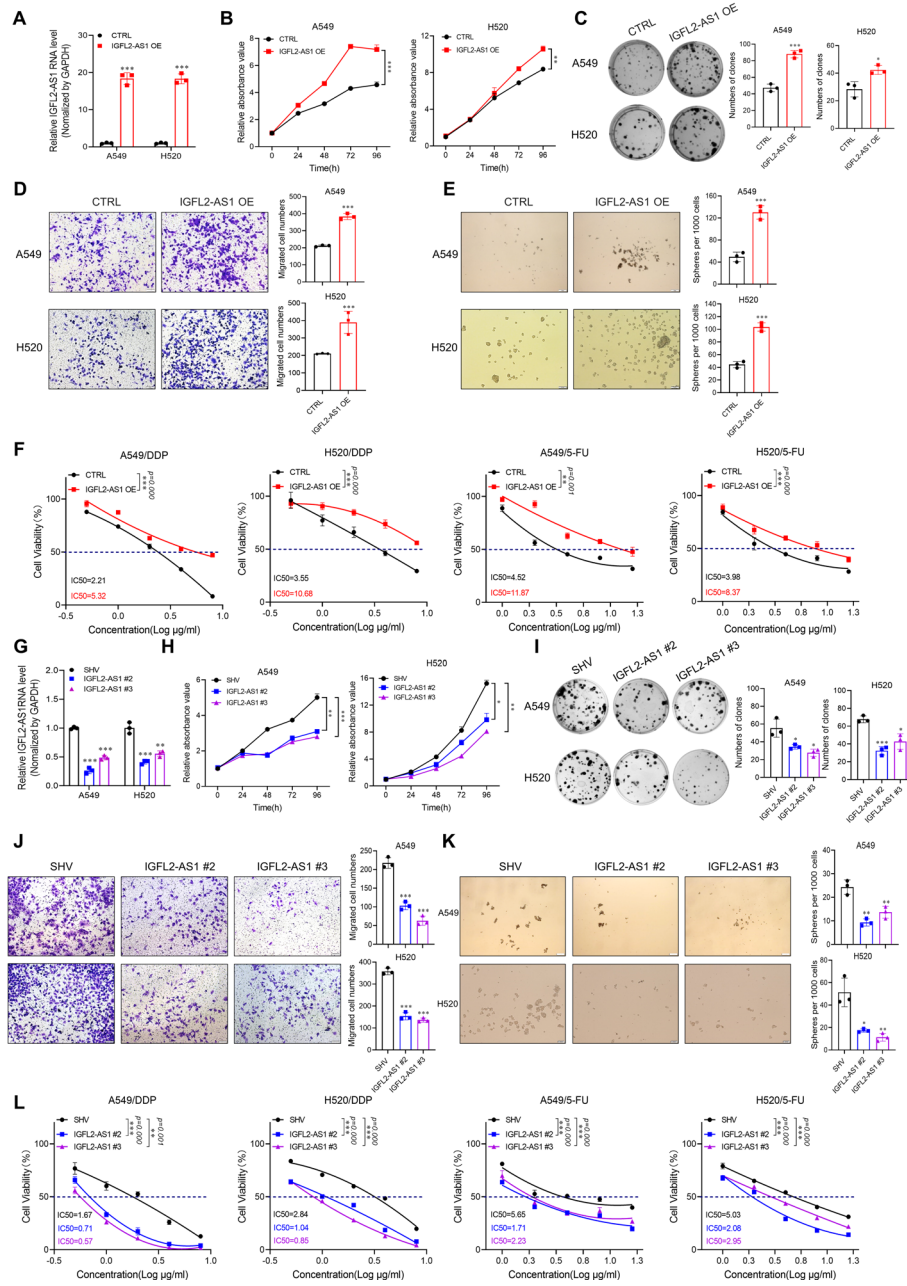


Fig. 2 IGFL2-AS1 modulates lung cancer proliferation, metastasis, stemness, and multidrug resistance in vitro. **A** Exogenous overexpression of *IGFL2-AS1* in lung cancer cells, as detected via qRT-PCR. **B** CCK8 assay of the proliferative capacity of A549 and H520 cells following *IGFL2-AS1* overexpression. **C** Colony formation assay and histogram quantification of lung cancer cells upon IGFL2-AS1 upregulation. **D** Transwell assay analysis of the effect of *IGFL2-AS1* overexpression on the migration capability of lung cancer cells; Scale bar, 50 μm. **E** Stemness features of lung cancer following IGFL2-AS1 overexpression. **F** CCK8 assay evaluating the effect of IGFL2-AS1 overexpression on lung cancer cell sensitivity to cisplatin (DDP) and 5-fluorouracil (5-FU) treatment. **G** shRNA-induced IGFL2-*AS1* downregulation in A549 and H520 lung cancer cells. **H**–**L** Effect of *IGFL2-AS1* knockdown on lung cancer cells: **H** proliferation, **I** colony formation, **J** migration (Scale bar, 50 μm), **K** stemness features (Scale bar, 50 μm), and **L** sensitivity to DDP and 5-FU treatment. All plots depict the mean \pm SD. Statistical analyses: two-tailed unpaired Student's t-test (**A**, **C**–**E**), one-way ANOVA with Dunnett's multiple-comparison test (**B**, **F**, **H**, and **L**). **P* < 0.05, ****P* < 0.01, *****P* < 0.001

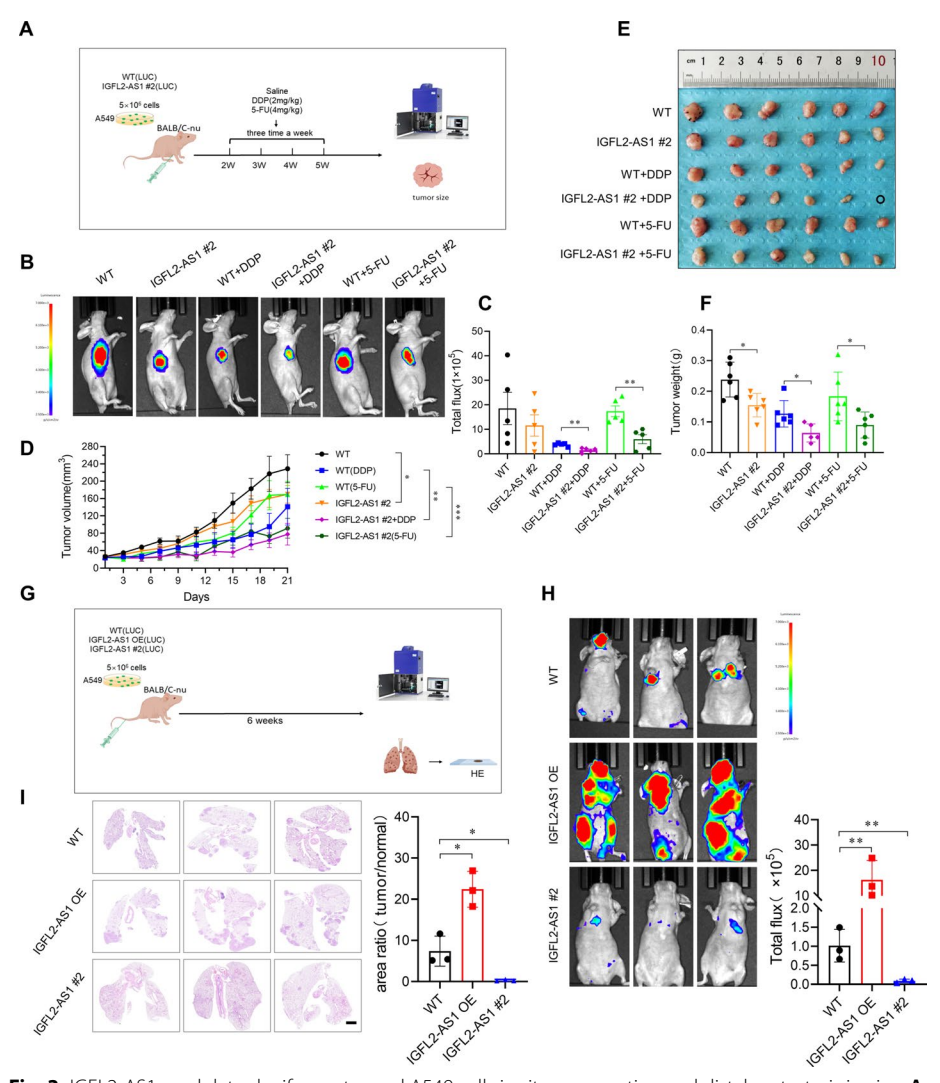


Fig. 3 IGFL2-AS1 modulates luciferase-tagged A549 cells in situ propagation and distal metastasis in vivo. **A** Schematic diagram illustrating subcutaneous lung cancer establishment and therapeutic administration. **B, C** Representative visualization of luciferase signals and histogram quantification of subcutaneously inoculated A549 cells upon *IGFL2-AS1* knockdown and/or chemotherapy. **D** Growth curves of tumor bulk in distinct groups. **E, F** Tumor bulk and weight upon *IGFL2-AS1* knockdown and/or chemotherapy (n=6 mice per group). **G** Schematic diagram illustrating lung cancer metastasis upon mice tail injection with A549 cells. **H** Visualization of luciferase signals and histogram quantification of A549 lung metastatic foci upon *IGFL2-AS1* overexpression or knockdown (n=3 mice per group). **I** Hematoxylin and eosin staining and quantification of lung metastasis upon *IGFL2-AS1* overexpression and knockdown. Scale bar, 1 mm. All plots present the mean \pm SD. Statistical analyses: two-tailed unpaired Student's t-test (**C, F**), two-way ANOVA with Dunnett's multiple-comparison test (**H, I**). *P<0.05, *P<0.01, **P<0.001

Knockdown experiments using two shRNA hairpins were performed, which effectively interfered with *IGFL2-AS1* transcription (Fig. 2G). *IGFL2-AS1* knockdown significantly inhibited the proliferation of lung cancer cells (Fig. 2H, I), reduced their migration capacity, and downregulated the expression of EMT-associated markers (Fig. 2J; Additional File 4: Fig. S2D, E). Moreover, *IGFL2-AS1* knockdown significantly

inhibited the growth of lung stemness spheres and markedly increased the sensitivity of lung cancer cells to DDP and 5-FU (Fig. 2K, L).

IGFL2-AS1 regulates lung cancer tumor bulk propagation and drug sensitivity in vivo

To assess the sensitization of lung cancer cells to chemotherapeutic drugs following IGFL2-AS1 genetic manipulation, A549 parental (WT) and IGFL2-AS1 knockdown cells tagged with luciferase were subcutaneously implanted into immunodeficient mice, followed by DDP or 5-FU administration (Fig. 3A). Fluorescent tumor imaging and quantification revealed that A549 cells with IGFL2-AS1 knockdown were more sensitive to DDP or 5-FU therapy than control cells (Fig. 3B, C; Additional File 5: Fig. S3A). The tumor growth curve demonstrated that IGFL2-AS1 knockdown alone inhibited tumor propagation and significantly increased the therapeutic efficacy of combined DDP and 5-FU (Fig. 3D). Tumor bulk imaging and weight quantification confirmed the function of IGFL2-AS1 as a lung cancer stimulator that contributes to drug resistance (Fig. 3E, F). Pathological staining for Ki67 (a proliferative marker), vimentin (an invasive marker), and sex-determining region Y-box 2 (SOX2, a stemness marker) confirmed that IGFL2-AS1 knockdown, either alone or in combination with DDP or 5-FU, reduced proliferation and stemness-related gene expression (Additional File 5: Fig. S3B). Notably, IGFL2-AS1 knockdown did not elicit observable side effects, as indicated by the body weight of the mice (Additional File 5: Fig. S3C).

A lung metastatic model was then established by injecting A549 cells into the tail vein of mice to assess the effect of IGFL2-AS1 on lung cancer distal metastasis (Fig. 3G). In vivo imaging and quantification demonstrated that IGFL2-AS1 promoted A549 metastasis to the lungs and brain, which are prevalent target organs of lung cancer, whereas *IGFL2-AS1* knockdown significantly diminished distal metastasis (Fig. 3H). H&E staining and quantification of metastatic foci in the lungs further revealed a strong modulatory effect of IGFL2-AS1 on distal metastasis (Fig. 3I). Collectively, these data suggest that IGFL2-AS1 promotes lung cancer proliferation, drug resistance, and metastasis in vivo, suggesting its pivotal role in lung cancer onset and progression.

C/EBPB positively regulates IGFL2-AS1 transcription in lung cancer

To elucidate how IGFL2-AS1 is consistently upregulated in drug-resistant cancer cells, the PROMO and GeneCards databases were screened for potential upstream modulators of IGFL2-AS1. Both databases predicted C/EBPβ and USF2 as the potential upstream regulators of IGFL2-AS1 (Fig. 4A). qRT-PCR and immunoblot analyses verified that C/EBPβ, but not USF2, was upregulated in DDP- and 5-FU-resistant cells compared with parental cells (Fig. 4B, C). To further evaluate whether IGFL2-AS1 was regulated by C/EBPβ, a C/EBPβ overexpression plasmid was constructed and validated in A549 and H520 cells at the protein level (Fig. 4D). qRT-PCR analysis further demonstrated that exogenous C/EBPβ overexpression significantly upregulated the *IGFL2-AS1* expression compared with the empty vector backbone group (Fig. 4E).

To investigate the potential mechanism by which C/EBP β modulates *IGFL2-AS1* expression, C/EBP β binding sites were predicted. C/EBP β , as a TF, can specifically bind the CCAAT sequence in the genome. Ten regions were predicted as being recognized by C/EBP β across the *IGFL2-AS1* genomic locus, representing potential binding sites

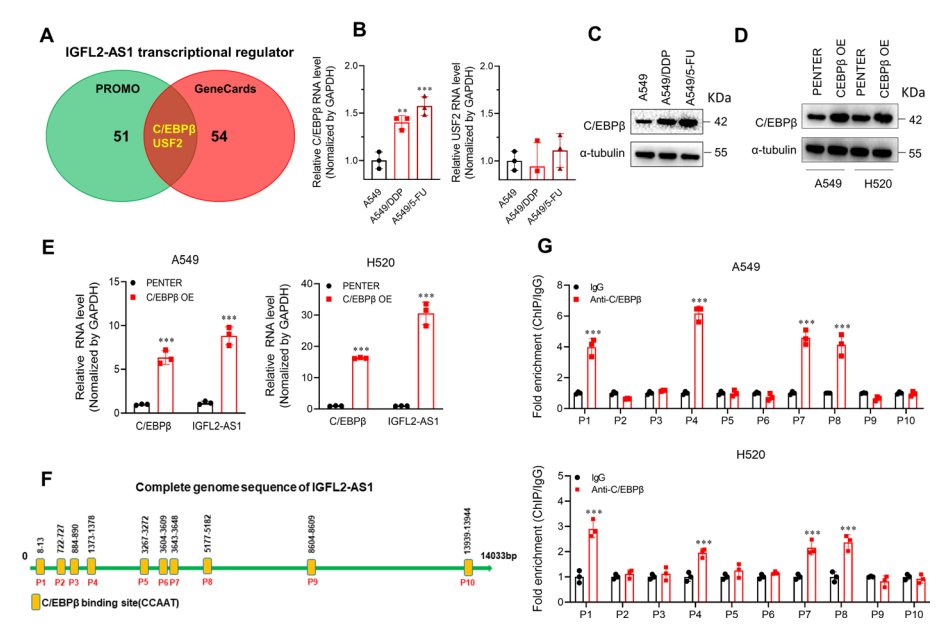


Fig. 4 *IGFL2-AS1* transcription is positively regulated by C/EBPβ in lung cancer cells. **A** Venn diagram illustrating bioinformatic prediction of transcriptional factors upstream of *IGFL2-AS1* by PROMO and GeneCards databases. **B** qRT-PCR analysis of C/EBPβ and USF2 expression in cisplatin (DDP) and 5-fluorouracil (5-FU)-resistant A549 cells compared with parental cells. **C** Immunoblotting of C/EBPβ expression in DDP- and 5-FU-resistant A549 cells. **D** Immunoblotting of exogenous C/EBPβ expression in A549 and H520 cells compared with the vector backbone. **E** qRT-PCR analysis of the effect of C/EBPβ activation on *IGFL2-AS1* transcription in lung cancer cells. **F** Predicted C/EBPβ binding regions on the *IGFL2-AS1* encoding region. **G** Binding sites of C/EBPβ on IGFL2-AS1 modulatory area validated by ChIP assay and qRT-PCR. All plots present the mean \pm SD. Statistical analyses: one-way ANOVA with Dunnett's multiple-comparison test (**B**), two-tailed unpaired Student's *t*-test (**E**, **G**). *P<0.05, **P<0.01, ***P<0.001

(Fig. 4F). Moreover, ChIP confirmed that the P1, P4, P7, and P8 regions of *IGFL2-AS1* were significantly enriched and bound by C/EBPβ in A549 and H520 cells (Fig. 4G).

IGFL2-AS1 modulates lung cancer cell migration and drug resistance via HSPA1A

RNA sequencing was performed using two lung cancer cell lines to further elucidate how IGFL2-AS1 exerts its oncogenic functions and mediates stemness-related drug resistance in lung cancer cells. Consistent with the RNA sequencing results of DDP-resistant A549 cells (Additional File 3: Fig. S1B), persistent oncogenic signaling cascades, including RAP1, were upregulated in *IGFL2-AS1*-overexpressing A549 and H520 cells (Additional File 6: Fig. S4A). Venn diagram analysis indicated that 90 genes overlapped between the two cell lines (Additional File 6: Fig. S4B), with *HSPA1A* being the most significantly influenced gene in both cell lines in response to *IGFL2-AS1* overexpression. Therefore, *HSPA1A* was selected for further functional and mechanistic investigation (Fig. 5A).

qRT-PCR and immunoblot analyses confirmed that HSPA1A was upregulated by *IGFL2-AS1* overexpression and downregulated by its knockdown in lung cancer cells (Fig. 5B–E). Furthermore, HSPA1A expression was aberrantly upregulated in DDP- and 5-FU-resistant A549 cells compared with the parental cells (Fig. 5F, G). To confirm that IGFL2-AS1 exerts its oncogenic function through HSPA1A, *HSPA1A*

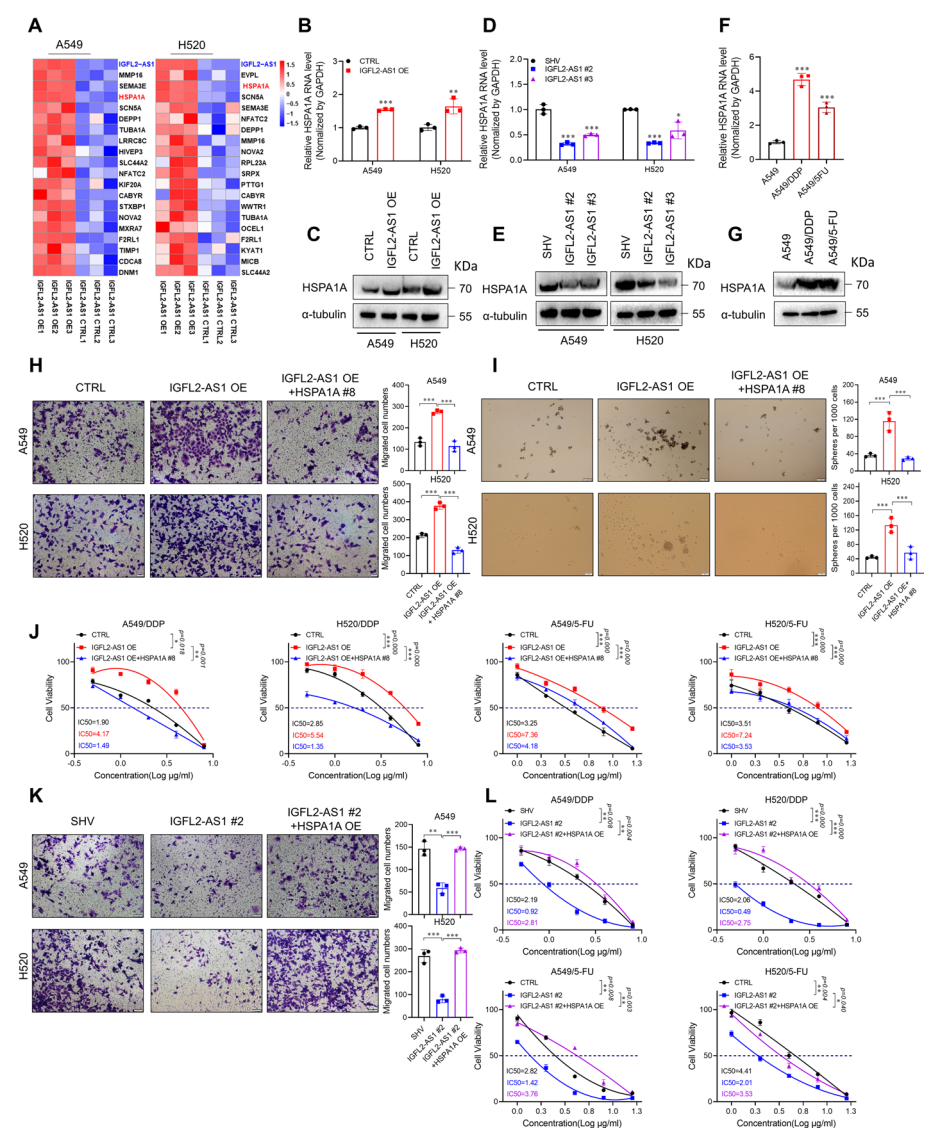


Fig. 5 IGFL2-AS1 modulates lung cancer cell migration and drug resistance via HSPA1A. A Heatmap showing the top 20 genes most significantly upregulated in IGFL2-AS1 overexpressing A549 and H520 cells compared with the corresponding parental control cells. B, C qRT-PCR and immunoblot analysis of the effect of IGFL2-AS1 overexpression on HSPA1A expression at the transcriptional (B) and translational (C) levels. D, E Effect of IGFL2-AS1 knockdown on HSPA1A expression at the transcriptional (D) and translational (E) levels. F, G HSPA1A expression in drug-resistant A549 cells detected via qRT-PCR (F) and immunoblot (G). H–J Effect of HSPA1A knockdown on H cellular migration promoted by IGFL2-AS1 overexpression (scale bar, 50 μm), I cellular stemness promoted by IGFL2-AS1 overexpression (scale bar, 50 μm), and J lung cancer cell resistance to cisplatin (DDP) and 5-fluorouracil (5-FU). K Effect of HSPA1A overexpression on the decreases in cellular migration (scale bar, 50 μm), and L resistance to DDP and 5-FU drug induced by IGFL2-AS1 knockdown. All plots present the mean ± SD. Statistical analyses: two-tailed unpaired Student's t-test (B), one-way ANOVA with Dunnett's multiple-comparison test (J, L). *P < 0.05, **P < 0.01, ***P < 0.001

knockdown and overexpression plasmids were constructed for rescue experiments. Immunoblot analyses verified the knockdown and overexpression efficacy in H520 cells, indicating that shRNAs #7 and #8 exhibited better suppression effects than the other plasmids; therefore, these plasmids were selected for double transfection

(Additional File 6: Fig. S4C). The EMT-related markers, Twist and Snail, were positively regulated, whereas E-cadherin was negatively modulated by HSPA1A in H520 cells (Additional File 6: Fig. S4D, E).

Transwell, wound healing, sphere formation, and drug resistance assays were performed for the two lung cancer cell lines overexpressing *IGFL2-AS1*, either alone or with *HSPA1A* knockdown double transfection. *HSPA1A* disruption significantly reversed the effects of *IGFL2-AS1* overexpression in promoting the migration, stemness, and drug resistance of lung cancer cells (Fig. 5H–J; Additional File 6: Fig. S4F). Moreover, exogenous *HSPA1A* overexpression significantly counteracted the effects of *IGFL2-AS1* knockdown in decreasing the migration and drug resistance of lung cancer cells (Fig. 5K, L; Additional File 6: Fig. S4G). These rescue experiments suggest that IGFL2-AS1 exacerbates migration and drug resistance in lung cancer cells primarily via HSPA1A.

IGFL2-AS1 stimulates HSPA1A expression by promoting YBX1 binding and activating transcription

To investigate how IGFL2-AS1 modulates the expression of HSPA1A in lung cancer cells, MS was performed following RNA pulldown experiments. A total of 35 proteins were specifically enriched in the *IGFL2-AS1* sense strand compared with the antisense strand (Fig. 6A). Protein localization analysis indicated that 11 of these proteins were primarily located in the nucleus, suggesting potential functional interactions with IGFL2-AS1. Among these, we focused on the RNA-binding protein HNRNPA1 (heterogeneous nuclear ribonucleoprotein A1) and TF YBX1, with essential roles in various cancers.

The interaction sites between *HNRNPA1*, *IGFL2-AS1*, and *HSPA1A* mRNA were predicted using the catRAPID database (Additional File 7: Fig. S5A, B). However, immunoblotting analysis following RNA pulldown and qRT-PCR after RIP failed to verify the

(See figure on next page.)

Fig. 6 IGFL2-AS1 stimulates HSPA1A expression by promoting YBX1 binding and activating transcription. A RNA pulldown followed by MS analysis of proteins bound specifically to the IGFL2-AS1 sense strand in A549 cells and their subcellular localization. **B** Direct interaction between YBX1 and the *IGFL2-AS1* sense strand, as verified by RNA pulldown followed by immunoblot assays in A549 and H520 cancer cells. C Direct interaction between YBX1 and IGFL2-AS1 validated by RNA immunoprecipitation (RIP) quantification (upper) and gel running (lower) precipitated by a YBX1 antibody compared with IgG (negative control). **D** Prediction of potential binding sites and mutated sequences of IGFL2-AS1 on YBX1 peptides and its conformational structure generated by the catRAPID website. **E** Binding capability of wild-type and mutated *IGFL2-AS1* with YBX1 protein in lung cancer cells detected via RNA pulldown assay and immunoblot. F Prediction of the interaction peptides in YBX1 with IGFL2-AS1 generated by catRAPID. G Interaction between IGFL2-AS1 and wild-type or truncated YBX1 detected via RIP upon Flag precipitation, followed by qRT-PCR (upper) and gel electrophoresis (lower) in H520 and 293T cells. H Interaction between IGFL2-AS1 and wild-type or truncated YBX1, as detected via RNA pulldown and immunoblot in H520 and 293T cells. I Predicted binding region of YBX1 on the HSPA1A promoter in lung cancer cells by JASPAR (upper) and validation with ChIP quantification (lower left) and gel electrophoresis (lower right). J Validation of the YBX1 binding sequence on the wild-type or mutated HSPA1A promoter (upper) using a luciferase reporter assay in 293T and H520 cells (lower). K Predicted binding region of YBX1 on the IGFL2-AS1 promoter by JASPAR (upper) and validation with ChIP quantification (lower left) and gel electrophoresis (lower right). L Validation of YBX1 binding sequence on the wild-type or mutated IGFL2-AS1 promoter (upper) using a luciferase reporter assay in 293T and H520 cells (lower). M Effect of IGFL2-AS1 downregulation on YBX1 to the HSPA1A promoter, as detected via ChIP. All plots depict the mean \pm SD. Statistical analyses: two-tailed unpaired Student's t-test (\mathbf{C} , \mathbf{G} , \mathbf{I} , \mathbf{K} and \mathbf{M}), one-way ANOVA with Dunnett's multiple-comparison test (J, L). *P<0.05, **P<0.01, ***P<0.001

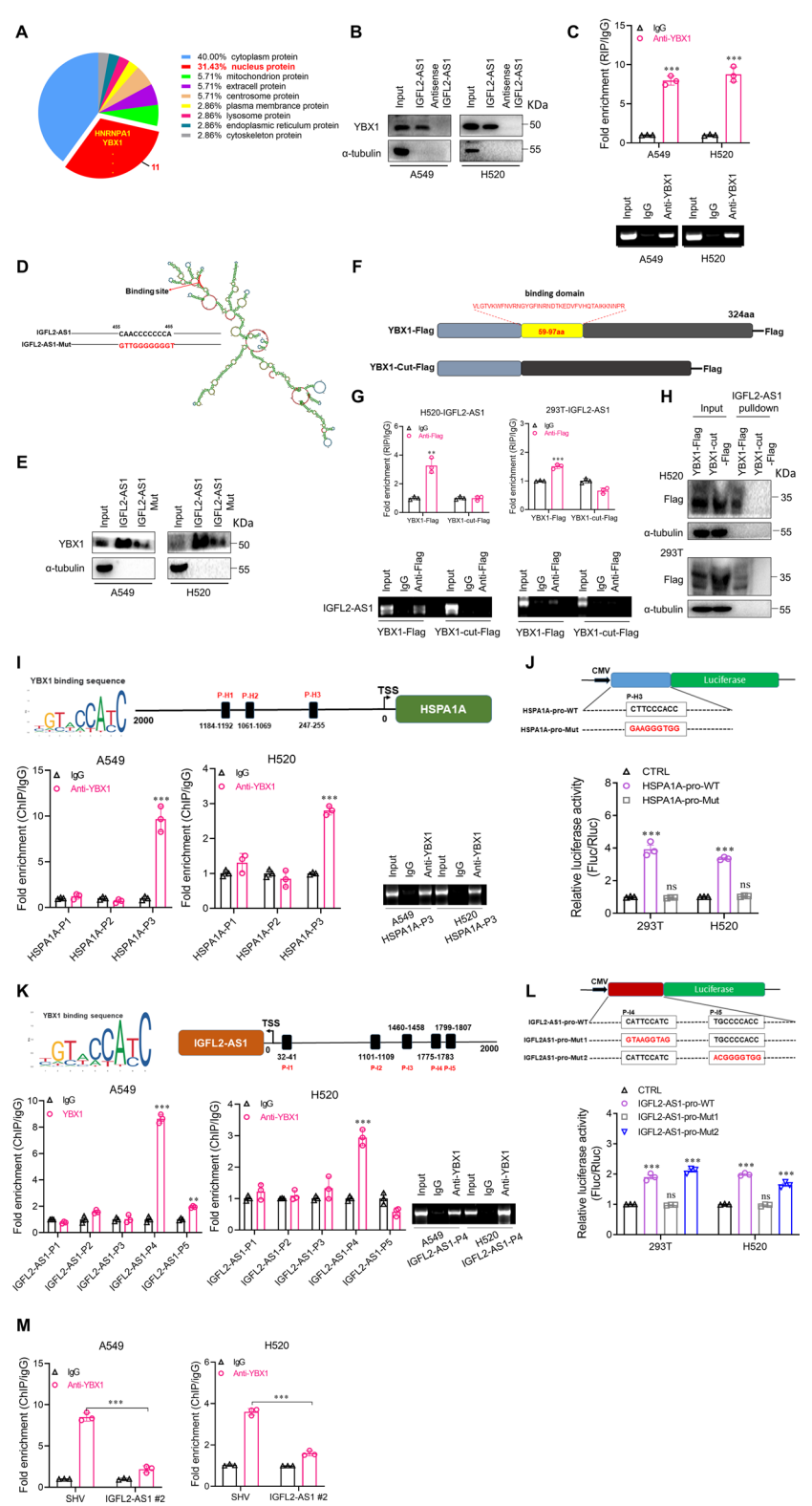


Fig. 6 (See legend on previous page.)

interaction between *IGFL2-AS1* and *HNRNPA1* in A549 cells (Additional File 7: Fig. S5C, D). Additionally, *IGFL2-AS1* downregulation did not impact the mRNA or protein levels of HNRNPA1, suggesting that IGFL2-AS1 did not function through HNRNPA1 (Additional File 7: Fig. S5E, F). Therefore, the second candidate, YBX1, was selected for further investigation.

RNA pulldown assays combined with immunoblotting verified the specific interaction between YBX1 and the sense strand of IGFL2-AS1 in A549 and H520 cells (Fig. 6B; Additional File 8: Fig. S6A). Furthermore, the RIP assay with the YBX1 antibody confirmed the binding between YBX1 to IGFL2-AS1 (Fig. 6C). The 455-465 region was predicted to be the precise binding site of YBX1 on IGFL2-AS1 using the CatRAPID (http://servi ce.tartaglialab.com/page/catrapid group) website (Fig. 6D; Additional File 8: Fig. S6B). RNA pulldown and immunoblotting revealed that, when the CAACCCCCCA binding sequence was mutated to CTTGGGGGGGT, the interaction between YBX1 and IGFL2-AS1 was significantly reduced (Fig. 6E). Moreover, the 59–97 amino acid region was predicted to be the binding domain of YBX1 for IGFL2-AS1 using the catRAPID website (Fig. 6F; Additional File 8: Fig. S6B). Vectors expressing full-length or truncated YBX1 peptides tagged with Flag were cloned. The RIP assay revealed that, compared with fulllength YBX1, the interaction between IGFL2-AS1 and truncated YBX1 was significantly abolished in H520 and 293 T cells, suggesting that the binding domain of YBX1 with IGFL2-AS1 is located in the 59-97 amino acid region (Fig. 6G). This was further confirmed via RNA pulldown assays. Compared with the positive control, IGFL2-AS1 precipitated FLAG-tagged wild-type YBX1 rather than the truncated peptide in H520 and 293 T cells (Fig. 6H).

In A549 and H520 cells, *YBX1* overexpression increased HSPA1A expression at both the mRNA and protein levels, whereas its downregulation decreased them (Additional File 8: Fig. S6C–E). Notably, IGFL2-AS1 expression was positively modulated by YBX1, suggesting the existence of a self-motivating loop in IGFL2-AS1 expression (Additional File 8: Fig. S6C, D).

The TF YBX1 was predicted to specifically bind to three promoter regions upstream of the HSPA1A transcription start site (TSS) (Fig. 6I). Following YBX1 precipitation, ChIP assay results demonstrated that the P-H3 region, rather than the P-H1 or P-H2 regions, of HSPA1A was bound by YBX1 in the two lung cancer cell lines (Fig. 6I). Luciferase assays confirmed that only wild-type promoter-driven luciferase was stimulated by YBX1, whereas the mutated sequence did not respond, similar to the vector backbone in 293T and H520 cells (Fig. 6J). These data suggest that YBX1 promotes HSPA1A transcription through direct interaction with the 247-255 region upstream of the TSS of HSPA1A. Similarly, the binding of YBX1 to the promoter sequence of IGFL2-AS1 was predicted and validated using a ChIP assay. The P-I4 region, 1175-1783 bp upstream of the TSS of IGFL2-AS1, interacted with YBX1 in A549 and H520 cells, whereas the P-I5 region, 1799-1807 bp upstream of the TSS, was significantly amplified compared with the IgG control only in A549 cells (Fig. 6K). Luciferase assays using 293 T and H520 cells verified that the P-I4 mutation eliminated luciferase activity compared with the vector control, whereas the P-I5 mutation had a negligible effect on promoter activity (Fig. 6L). These data suggest that YBX1 promotes the transcription of IGFL2-AS1 by specifically interacting with and activating the 1175–1783-bp region upstream of the TSS.

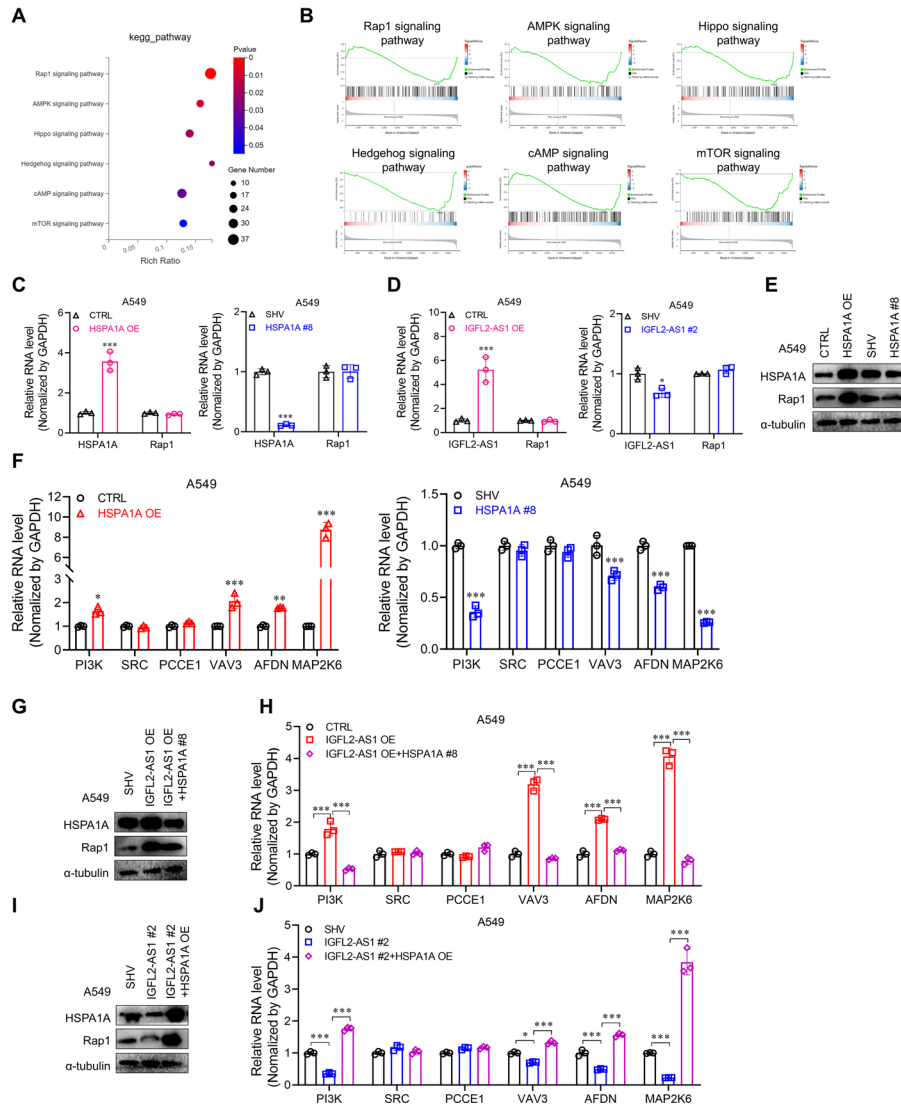
Given that lncRNAs can act as guide RNAs to facilitate the binding between TFs and target genes, the interaction between YBX1 and the P-H3 region of the *HSPA1A* promoter was assessed following *IGFL2-AS1* knockdown. ChIP assay results demonstrated that IGFL2-AS1 knockdown significantly inhibited the interaction between YBX1 and the P-H3 region of the *HSPA1A* promoter compared with control A549 and H520 cells (Fig. 6M). The results further indicated that IGFL2-AS1 does not directly influence YBX1 expression at the RNA or protein levels (Additional File 8: Fig. S6F, G). These findings suggest that IGFL2-AS1 promotes *HSPA1A* transcription by increasing the binding of YBX1 to its promoter without affecting YBX1 levels.

HSPA1A positively modulates oncogenic pathways and negatively regulates tumor-suppressing signaling cascades

As our in vitro and in vivo studies consistently revealed that HSPA1A has an essential role in mediating the propagation, migration, and drug resistance of lung cancer cells, RNA sequencing was performed to explore its downstream targets. HSPA1A knockdown repressed multiple oncogenic pathways, including RAP1, AMPK, YAP, Hedgehog, cyclic adenosine monophosphate (cAMP), and Hedgehog hallmarks, while upregulating P53 and apoptotic signaling cascades (Fig. 7A; Additional File 9: Fig. S7B). Heatmap and gene set enrichment analyses confirmed the inhibition of downstream signaling in the RAP1 cascade, which was activated as the top targeted pathway and activation of anticancer hallmarks following HSPA1A knockdown (Fig. 7B; Additional File 9: Fig. S7A, C, D). Annexin V/PI staining verified that both HSPA1A and IGFL2-AS1 knockdown significantly promoted apoptotic signaling in lung cancer cells (Additional File 9: Fig. S7E). Moreover, qRT-PCR and immunoblot analyses revealed that genetic manipulation of HSPA1A or IGFL2-AS1 affected RAP1 expression at the protein, but not transcriptional, level in A549 cells (Fig. 7C-E). qRT-PCR analysis also confirmed that four of six candidate genes, including PI3K, VAV3, AFDN, and MAP2K6, but not SRC or PCCE1, were positively modulated by HSPA1A (Fig. 7F). Moreover, the simultaneous transduction of IGFL2-AS1-overexpressing and HSPA1A-knockdown plasmids confirmed that IGFL2-AS1 upregulated RAP1 protein levels by downregulating HSPA1A (Fig. 7G-J). qRT-PCR analysis confirmed that IGFL2-AS1 promoted downstream targets, including PI3K, VAV3, AFDN, and MAP2K6, by activating HSPA1A (Fig. 7G-J).

Pharmacological inhibition of HSPA1A restores chemotherapy sensitivity and attenuates lung cancer cell metastasis in vivo

As HSPA1A is the key terminal executor of the IGFL2-AS1/YBX1/HSPA1A positive loop that promotes lung cancer progression, an HSPA1A inhibitor (VER155008) was used alone or in combination with low-dose conventional chemotherapeutics in a mouse model (Fig. 8A). Time-course luminescent imaging and growth curves demonstrated that the slight reduction in subcutaneous tumor growth achieved by low-dose DDP, particularly 5-FU, was remarkably enhanced by combination therapy with the HSPA1A inhibitor (Fig. 8B, C; Additional File 10: Fig. S8A). The tumor bulk and weight confirmed that VER155008 synergistically enhanced the antitumor efficacy of low-dose DDP and 5-FU in a subcutaneously implanted lung cancer model (Fig. 8D, E). Consistent with this, IHC staining for Ki67 indicated that combined VER155008



and DDP or 5-FU resulted in the lowest proliferative capacity compared with the monotherapy or saline-treated control groups (Additional File 10: Fig. S8B). Furthermore, IHC staining validated the potent repression of HSPA1A protein expression following VER155008 administration alone or in combination with chemotherapeutic

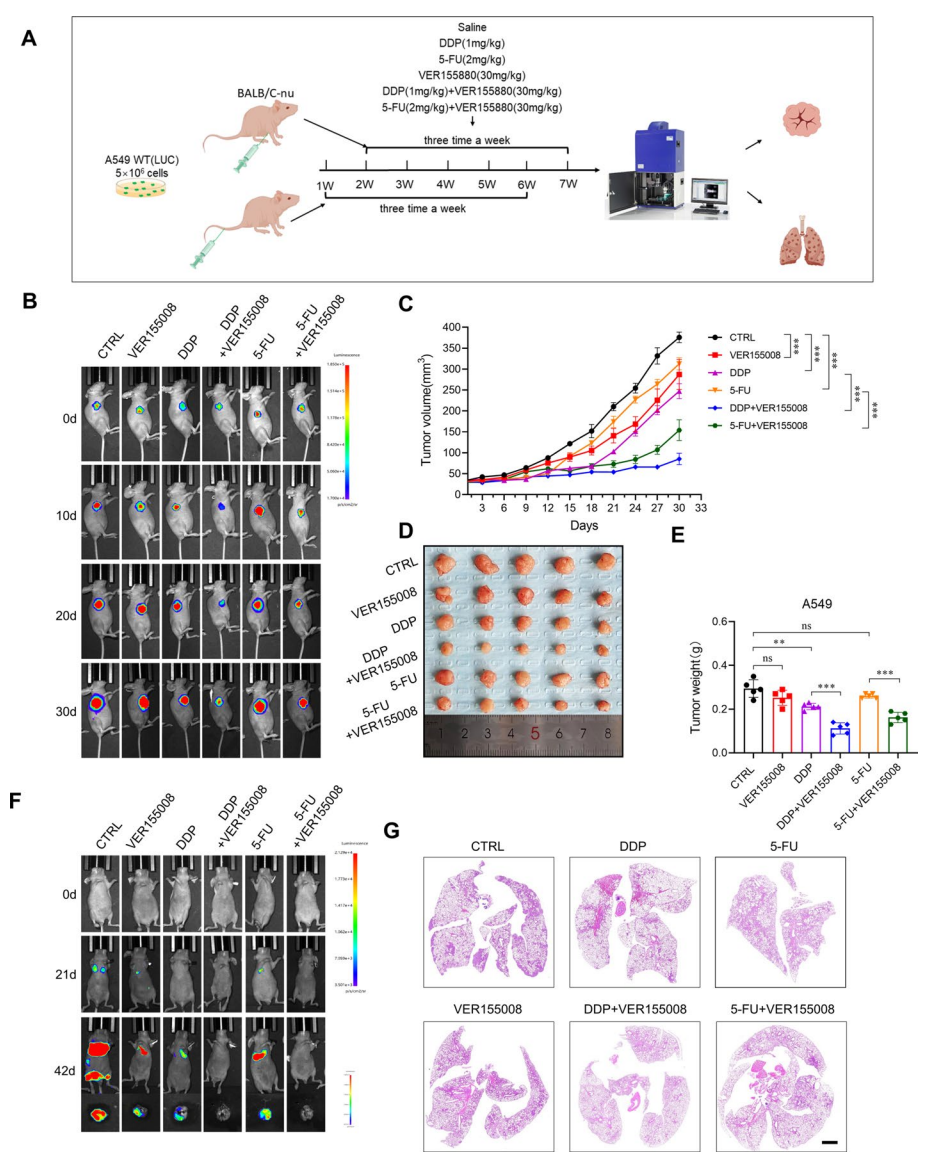


Fig. 8 In vivo therapeutic intervention of HSPA1A enhances the sensitivity of lung cancer to chemotherapies and attenuates distal organ metastasis. **A** Schematic workflow of the mouse model establishment and drug administration. **B** Representative images of tumor luminescent signal upon HSPA1A inhibitor, cisplatin (DDP), or 5-fluorouracil (5-FU) monotherapy or combinational intervention at different time points. **C** Growth curve of subcutaneously implanted A549 tumor bulk upon various therapies (DDP vs. DDP + VER155008, P = 0.000; 5-FU vs. 5-FU + VER155008, P = 0.000). **D**, **E** Tumor images (**D**) and weight quantification (**E**) upon indicated treatment (DDP vs DDP + VER155008, P = 0.000; 5-FU vs. 5-FU + VER155008, P = 0.000). **F** Representative images of tumor luminescent signal after tail injection of luciferase-tagged A549 cells at different time points. **G** Representative hematoxylin and eosin staining of whole lung sections in groups. Scale bar, 1 mm. All plots present the mean \pm SD (n = 5 mice per group). Statistical analyses: two-way ANOVA with Dunnett's multiple-comparison test (**C**), two-tailed unpaired Student's t-test (**E**). *t < 0.05, *t < 0.01, *t < 0.001

drugs (Additional File 10: Fig. S8C). Luciferase-monitored lung metastasis after tail injection demonstrated that VER155008 alone reduced A549 metastasis in distal organs, particularly the lungs, and further enhanced the antimetastatic efficacy of DDP and 5-FU (Fig. 8F; Additional File 11: Fig. S9). Moreover, HE staining revealed

that the metastatic foci in the lung were significantly reduced in the VER155008 monotherapy group and abolished in the combination groups (Fig. 8G). Collectively, these results indicate that HSPA1A inhibition effectively inhibits lung metastasis and enhances the sensitivity of lung cancer cells to chemotherapeutic drugs in vivo.

IGFL2-AS1/YBX1/HSPA1A expression in clinical specimens and correlation with the prognosis of patients with lung cancer

Tissue microarray staining revealed aberrant upregulation of IGFL2-AS1 expression in lung cancer specimens compared with paired adjacent tissues (Fig. 1G). Moreover, microarray analysis of the same lung cancer tissues revealed that YBX1 was significantly activated in paired lung cancer specimens, serving as a strong indicator of poor prognosis based on OS (Fig. 9A–C). Similarly, IHC staining of the microarray indicated abnormal stimulation of HSPA1A in malignant lung cancer tissues compared with benign paired normal lung specimens and significantly correlated with poor OS (Fig. 9D–F). Correlation analysis demonstrated a positive association among the expression of IGFL2-AS1/YBX1/HSPA1A protein in lung cancer tissues, further supporting the existence of an IGFL2-AS1/YBX1/HSPA1A positive loop in lung cancer initiation (Fig. 9G). Finally, to preliminarily explore whether the IGFL2-AS1/YBX1/HSPA1A signature serves as an effective indicator of lung cancer prognosis, Kaplan–Meier curve analysis was performed using a tissue microarray cohort (Additional File 1: Table 4), revealing that combining IGFL2-AS1 and YBX1 represents a potent indicator of poor prognosis in patients with lung cancer (Fig. 9H).

On the basis of the functional and mechanistic investigation, schematics of the mode of action were generated, illustrating drug resistance and metastasis in lung cancer progression (Fig. 10). In resistant lung cancer cells, the aberrant stimulation of IGFL2-AS1 driven by C/EBPβ induced *HSPA1A* transcription by facilitating YBX1 interaction and activation as a TF. Specifically, YBX1 promoted IGFL2-AS1 transcription to form a positive feedback loop, while HSPA1A initiated multiple downstream cancer-related signaling cascades, leading to drug resistance and metastasis in lung cancer. Therefore, pharmacological blockade of the IGFL2-AS1/YBX1/HSPA1A axis may serve as a potential therapeutic option for patients with chemo-drug-resistant lung cancer, and the upregulation of this axis may represent a diagnostic marker of lung cancer.

Discussion

Drug resistance in cancer is accompanied by multiple malignant traits, including proliferative progression, metastasis, and stemness, making it a major obstacle for effective cancer therapy [26]. In this study, through high-throughput screening and functional validation both in vitro and in vivo, we identified a novel IGFL2-AS1/HSPA1A/RAP1 cascade stimulated by YBX1 to promote drug resistance and metastasis in lung cancer. Pharmacological disruption of this cascade effectively restored the sensitivity of lung cancer cells to conventional chemotherapeutic regimens and inhibited distal metastasis. Moreover, the expression of YBX1, IGFL2-AS1, and HSPA1A was positively correlated with lung cancer specimens and predicted poor patient prognosis.

IGFL2-AS1 is significantly upregulated in renal cell carcinoma and breast cancer, highlighting its potential diagnostic value in clinical settings [27, 28]. In colon cancer,

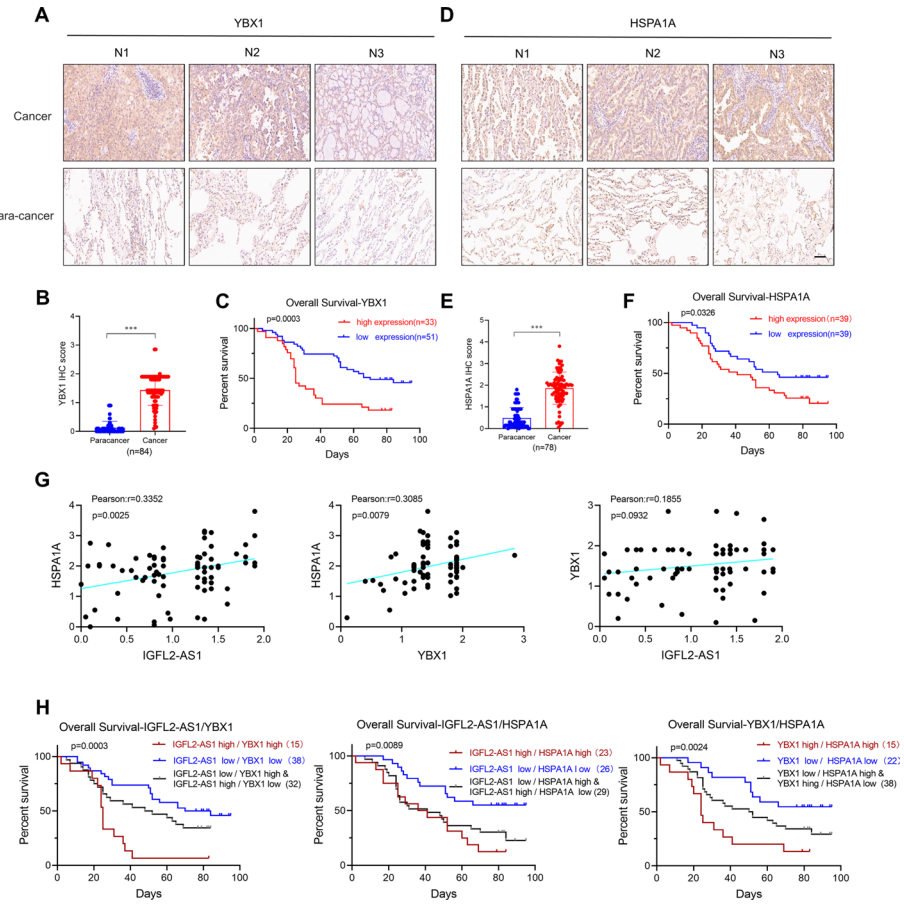


Fig. 9 Expression levels of the IGFL2-AS1/YBX1/HSPA1A axis in lung cancer and its clinical prognostic significance. **A** Representative image of YBX1 staining in tissue microarray, detected using immunohistochemistry staining. Scale bar, 100 μm. **B** Quantification of YBX1 protein level in paired lung cancer and adjacent specimens. **C** Kaplan–Meier curve of overall survival based on YBX1 expression in lung cancer tissues. The red line represents the high-expression group (n = 33, H-score > 1.425), while the blue line denotes the low-expression group (n = 51, H-score ≤ 1.425). **D** Representative picture of HSPA1A staining in tissue microarray detected via immunohistochemistry staining. Scale bar, 100 μm. **E** Quantification of HSPA1A protein expression in paired lung cancer and adjacent specimens. **F** Kaplan–Meier curve of overall survival based on HSPA1A expression level in lung cancer tissues. The red line represents the high-expression group (n = 40, H-score > 1.975), while the blue line denotes the low-expression group (n = 38, H-score ≤ 1.975). **G** Correlation of expression level among IGFL2-AS1/HSPA1A/YBX1 proteins in lung cancer specimens. **H** Overall survival curve of patients with lung cancer based on combinational markers of the IGFL2-AS1/HSPA1A/YBX1 signaling cascade. All plots present the mean \pm SD (total n = 84 for YBX1 analysis, n = 78 for HSPA1A analysis). Statistical analyses: two-tailed paired Student's t-test (**B**, **E**), log-rank (Mantel–Cox) test (**C**, **F** and **H**), and Spearman test (**G**). *tP<0.05, *tP<0.01, *tP<0.001

IGFL2-AS1 serves as an unfavorable independent prognostic marker, and its knockdown markedly reduces colon cancer cell proliferation and metastasis [29]. Our data further corroborated the oncogenic role of IGFL2-AS1 and its association with poor prognosis in lung cancer. Although IGFL2-AS1 is upregulated in cervical squamous cell carcinoma (SCC) compared with adenocarcinoma (ADC) [30], a similar distinction was not observed in the present study between SCC and ADC. In colorectal cancer cells, IGFL2-AS1 is predominantly expressed in the cytoplasm and promotes the malignant proliferation and invasion of neoplastic cells by acting as an RNA sponge [31, 32]. IGFL2-AS1 also functions as a competing endogenous RNA to facilitate the progression of gastric

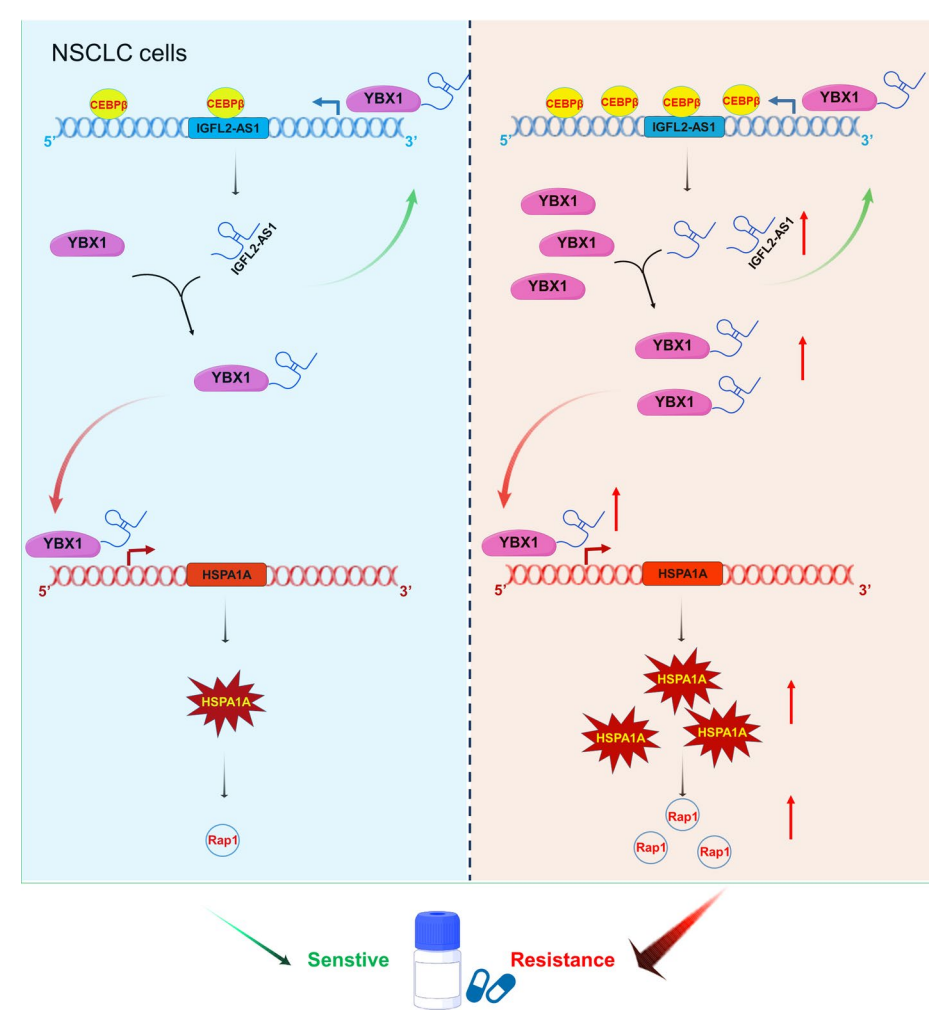


Fig. 10 Mechanistic illustration

cancer and tongue SCC [33, 34]. In contrast, our data indicated that IGFL2-AS1 is primarily localized within the nucleus of lung cancer cells. Mechanistically, IGFL2-AS1 activated downstream oncogenic cascades by acting as a protein scaffold and guiding the TF YBX1 to the target gene *HSPA1A*. Consistent with our findings, IGFL2-AS1 has been reported to be expressed in the cytoplasm and nucleus of basal-like breast cancer cells and to promote the transcription of its neighbor gene *IGFL1* by guiding the KLF5/TEAD4 complex to its promoter [35].

IGFL2-AS1 contributes to the development of resistance to multiple therapies in various cancers. For example, IGFL2-AS1 has been shown to lead to radio-resistance in colorectal cancer by activating the AKT pathway [36]. In clear cell renal cell carcinoma, IGFL2-AS1/TWIST1 signaling contributes to pazopanib resistance via vascular mimicry formation [37]. In renal cell carcinoma, IGFL2-AS1 packaged in extracellular vesicles promotes resistance to sunitinib by regulating TP53–INP2-mediated autophagy [38]. In the present study, functional exploration studies demonstrated that IGFL2-AS1 repression attenuated the malignant features of neoplastic cells, including proliferation, drug resistance, metastasis, and stemness, serving as a potential target for nucleic acid drugs

in lung cancer therapy. Notably, IGFL2-AS1 knockdown increased the sensitivity of lung cancer cells to chemotherapy, including DDP and 5-FU, but not to targeted therapies such as epidermal growth factor receptor (EGFR) inhibitors. These data suggest that the downstream targets of IGFL2-AS1 are not involved in or do not interact with the EGFR cascade.

In the present study, YBX1 was aberrantly upregulated in NSCLC specimens and significantly predicted poor patient prognosis. YBX1, a DNA- and RNA-binding protein upregulated in many cancer types, acts as an oncogene [8]. In the cytoplasm, YBX1 directly interacts with the lncRNA EVADR and facilitates the translation of EMT-associated markers, promoting distal metastasis of colorectal cancer [39]. Similarly, YBX1 binds to the lncRNA MILIP to promote the invasion and distal metastasis of clear cell renal cell carcinoma via translational activation of Snail [40]. As an m⁵C reader, YBX1 is indispensable for gefitinib resistance in NSCLC cells [41]. However, YBX1 has also been found to be enriched in the cytoplasm of lung cancer cells, where it acts as a scaffold for circRNAs to exert an inhibitory effect on tumor progression [42]. In the nucleus, YBX1 acts as an oncogenic TF that promotes the progression of pancreatic adenocarcinoma [43]. YBX1 also interacts with the -1480 to -1476 region of the MUC1 promoter to promote NSCLC cell progression and stemness [44, 45]. Similarly, YBX1 promotes NSCLC metastasis by interacting with the -358 to -350 region of the HOXC8 promoter and upregulates transcription [46]. In the present study, we found that YBX1 interacted with the promoter of its downstream target HSPA1A at distinct sequences and with IGFL2-AS1 at the 59–97 aa region, further confirming its role as an oncogenic TF.

The HSP70 family is upregulated in various cancer types and contributes to chemotherapy resistance and programmed cell death [47]. For example, circulating HSP70 levels are significantly lower in the plasma of patients with lung cancer than in healthy individuals [48]. HSP70 exhibits higher sensitivity and specificity than conventional carcinoembryonic antigen (CEA) and carbohydrate antigen (CA) 19-9 in early-stage (I and II) lung cancer, serving as a potential diagnostic marker [48]. Additionally, HSPA1A downregulation in mycosis fungoides, a type of cutaneous T-cell lymphoma, compared with benign conditions has been shown to be strongly correlated with disease progression and to serve as a marker of poor prognosis [22]. However, HSPA1A expression has been found to be elevated in lung adenocarcinoma (LAD), and its repression has been shown markedly inhibits tumor progression in ARID2-deficient LAD subtypes [49]. Our data indicated that HSPA1A was aberrantly upregulated in lung cancer specimens and predicted an unfavorable OS. Moreover, our functional assays confirmed the oncogenic role of HSPA1A in lung cancer cells. RNA sequencing revealed that HSPA1A stimulated multiple signaling cascades that promoted cancer progression, such as RAP1, AMPK, and Hedgehog, while inhibiting P53-related apoptosis signaling pathways. We have previously reported that Hedgehog components are upregulated in lung cancer specimens, and inhibition of their key terminal TF, GLI1/2, attenuates stemness-associated features, including multidrug resistance and distal metastasis [17, 18]. Notably, RAP1 contributes to lung cancer metastasis and progression [50]. For example, the expression of cytoplasmic RAP1 is higher in high-grade NSCLC specimens than in low-grade NSCLC specimens, and RAP1 inhibition enhances the sensitivity of lung cancer cells to DDP treatment via the NF-κB cascade [51]. Overall, the modulation of multiple classic

tumor-related pathways highlights the essential role of HSPA1A in lung cancer progression, positioning it as a promising therapeutic target in clinical settings.

Although the role of lncRNAs in NSCLC drug resistance has been previously established, the IGFL2-AS1/YBX1/HSPA1A axis described in the present study functions by activating multiple oncogenic cascades while suppressing apoptotic signaling, highlighting its potential role in distinct therapeutic strategies including radiotherapy, targeted therapy, and immune therapy. The lncRNA HOTAIR primarily exerts its oncogenic effects through H3k27me3 epigenetic modification, leading to the silencing of tumor suppressor genes. MALAT 1 acts as a competing endogenous RNA by absorbing miR-NAs to enhance the expression of target oncogenes. Moreover, MEG suppresses cancer progression via these two mechanisms [52-54]. Unlike these previously identified lncRNAs, IGFL2-AS1, which acts as a guide RNA, stimulates HSPA1A expression by promoting TF YBX1 binding and activating its transcription, along with multiple downstream oncogenic signaling cascades. Nevertheless, the present study is limited by its cell-intrinsic approach, relying primarily on cell line models and mouse xenografts, which may not fully recapitulate the human tumor microenvironment. Future studies should incorporate transgenic mouse models or organoid-immune cell coculture systems to validate our findings in a more clinically relevant context.

Conclusions

This study highlights the pivotal role of the IGFL2-AS1/YBX1/HSPA1A axis in promoting chemoresistance and metastasis in NSCLC. Our results indicate that targeting this axis could provide a novel therapeutic approach to overcome drug resistance in lung cancer and improve patient prognosis. Further research is warranted to explore the clinical applications of these findings and to develop effective strategies for targeting this pathway in lung cancer therapy.

Abbreviations

DDP Cisplatin
SR Secondary resistant
PR Primary resistant
PC Parental A549 cells
5-FU 5-Fluorouracil

HBEC Human bronchial epithelial cell FISH Fluorescent in situ hybridization

IGFL2-AS1 OE PLent-EF1a-FH-CMV-copGFP-P2A-Puro-IGFL2-AS1-OE overexpressing lentiviral vectors

CTRL PLent-EF1a-FH-CMV-copGFP-P2A-Puro vector backbone

IC₅₀ Half-maximal inhibitory concentration

IGFL2-AS1 #2 or #3 PLent-U6-shRNA-CMV-copGFP-P2A-Puro-shRNA #2 or #3, shRNA lentiviral vectors

SHV PLent-U6-shRNA-CMV-copGFP-P2A-Puro vector backbone

Supplementary Information

The online version contains supplementary material available at https://doi.org/10.1186/s11658-025-00808-5.

| ١ | | |
|---|--------------------|--|
| | Additional file 1. | |
| | Additional file 2. | |
| | Additional file 3. | |
| | Additional file 4. | |
| | Additional file 5. | |
| | Additional file 6. | |
| | | |

| Additional file 7. | ١ |
|---------------------|---|
| Additional file 8. | |
| Additional file 9. | |
| Additional file 10. | |
| Additional file 11. | |

Acknowledgements

We thank Prof. Zhao Qi for providing guidance on the bioinformatics analysis.

Author contributions

JD, AS, and FN designed and supervised the study. HD, YX, and CL performed the experiments. JQ, NZ, and JD helped with the data analysis. JQ, WL, and YY conducted bioinformatics analyses. HD, CL, and FW performed in vitro experiments. HD, YX, BC, and WC performed in vivo experiments. WL, JD, HD, and YX edited the manuscript. All the authors have reviewed and approved the final manuscript.

Funding

This study was supported by the National Natural Science Foundation of China (31900441, 82373097, 82172565, and 81502937 to JD, JD, and WWL), Natural Science Foundation of Shandong Province (ZR2019MC026, ZR2023QH080, and WSR2023085 to JD, FW, and CAS), Funds of Shandong Traditional Chinese Medicine Science and Technology Development Project (2019-0514 to JD), Qilu Outstanding Young Talents in Health Project and Taishan Scholarship (to JD), Ministry of Education "Chunhui" plan international cooperation project (HZKY20220459 to JD), Research Foundation of Binzhou Medical University Hospital (2022-01 and BY2022KJ64 to FW and BJC); Research foundation of Johannes Kepler University (2020–2026 to YY, BERM16108001; Tyle Private Foundation to CAS).

Availability of data and materials

The datasets generated in this study are available from the corresponding author upon request. All authors have agreed to publish this manuscript.

Declarations

Ethics approval and consent to participate

The procedures for animal care and use have been approved by the Animal Experimental Research Ethics Committee of Binzhou Medical University Hospital on 14 October 2022 (approval no. 20221014-101). Animal care and procedures comply with the ethical guidelines issued by the Ethics and Animal Welfare Committee of the International Scientific Committee on Experimental Animals (ICLAS) on 6/6/2013.

Consent for publication

Not applicable.

Competing interests

The authors declare no competing interests.

Author details

¹Department of Respiratory and Critical Care Medicine, Binzhou Medical University Hospital, 661 Huanghe Second Road, 256600 Binzhou, People's Republic of China. ²Medical Research Center, Binzhou Medical University Hospital, 256600 Binzhou, People's Republic of China. ³Department of Oncology, Binzhou Medical University Hospital, 256600 Binzhou, People's Republic of China. ⁴Department of Gynecology, Binzhou Medical University Hospital, 256600 Binzhou, People's Republic of China. ⁵Faculty of Medicine, Johannes Kepler University Linz, Altenberger Strasse 69, 4040 Linz, Austria. ⁶Department of Pharmacy, Binzhou Medical University Hospital, 256600 Binzhou, People's Republic of China. ⁷Johannes Kepler University, Altenbergerstraße 69, 4040 Linz, Austria. ⁸Charité—Universitätsmedizin Berlin, Freie Universität Berlin, Humboldt-Universität Zu Berlin, and Berlin Institute of Health, Medical Department of Hematology, Oncology and Tumor Immunology, and Molekulares Krebsforschungszentrum—MKFZ, Campus Virchow Klinikum, 13353 Berlin, Germany. ⁹Max-Delbrück-Center for Molecular Medicine in the Helmholtz Association, Robert-Rössle-Straße, 1013125 Berlin, Germany. ¹⁰Department of Hematology and Internal Oncology, Kepler University Hospital, Krankenhausstraße 9, 4020 Linz, Austria.

Received: 8 February 2025 Accepted: 29 September 2025

Published online: 07 November 2025

References

- 1. Siegel RL, Miller KD, Wagle NS, Jemal A. Cancer statistics, 2023. CA Cancer J Clin. 2023;73(1):17–48.
- 2. Vasan N, Baselga J, Hyman DM. A view on drug resistance in cancer. Nature. 2019;575(7782):299–309.
- Bushweller JH. Targeting transcription factors in cancer—from undruggable to reality. Nat Rev Cancer. 2019;19(11):611–24.

- Li YW, Azmi AS, Mohammad RM. Deregulated transcription factors and poor clinical outcomes in cancer patients. Semin Cancer Biol. 2022;86:122–34.
- Tolomeo M, Grimaudo S. The, "Janus" role of C/EBPs family members in cancer progression. Int J Mol Sci. 2020;21(12):4308.
- Long HC, Li YY, Wang HJ, Guo BX, Song SY, Zhe XY, et al. C/EBPbeta expression decreases in cervical cancer and leads to tumorigenesis. BMC Cancer. 2023;23(1):79.
- 7. Sterken BA, Ackermann T, Muller C, Zuidhof HR, Kortman G, Hernandez-Segura A, et al. C/EBPbeta isoform-specific regulation of migration and invasion in triple-negative breast cancer cells. NPJ Breast Cancer. 2022;8(1):11.
- 8. Prabhu L, Hartley A-V, Martin M, Warsame F, Sun E, Lu T. Role of post-translational modification of the Y box binding protein 1 in human cancers. Genes Dis. 2015;2(3):240–6.
- Wajapeyee N, Gupta R. Epigenetic alterations and mechanisms that drive resistance to targeted cancer therapies. Cancer Res. 2021;81(22):5589–95.
- 10. Herman AB, Tsitsipatis D, Gorospe M. Integrated Incrna function upon genomic and epigenomic regulation. Mol Cell. 2022;82(12):2252–66.
- 11. Liu KS, Gao L, Ma XS, Huang JJ, Chen J, Zeng LL, et al. Long non-coding RNAs regulate drug resistance in cancer. Mol Cancer. 2020;19(1):54.
- 12. Chen BQ, Dragomir MP, Yang C, Li QQ, Horst D, Calin GA. Targeting non-coding RNAs to overcome cancer therapy resistance. Signal Transduct Target Ther. 2022;7(1):121.
- 13. Zhang XY, Xie K, Zhou HH, Wu YW, Li C, Liu YT, et al. Role of non-coding RNAs and RNA modifiers in cancer therapy resistance. Mol Cancer. 2020;19(1):47.
- 14. Grillone K, Ascrizzi S, Cremaschi P, Amato J, Polerà N, Croci O, et al. An unbiased lncRNA dropout CRISPR-Cas9 screen reveals RP11-350G8.5 as a novel therapeutic target for multiple myeloma. Blood. 2024;144(16):1705–21.
- 15. He WM, Liang BS, Wang CL, Li SW, Zhao Y, Huang Q, et al. MSC-regulated IncRNA MACC1-AS1 promotes stemness and chemoresistance through fatty acid oxidation in gastric cancer. Oncogene. 2019;38(23):4637–54.
- Cheng ZA, Lu CL, Wang H, Wang N, Cui SH, Yu CT, et al. Long noncoding RNA LHFPL3-AS2 suppresses metastasis of non-small cell lung cancer by interacting with SFPQ to regulate TXNIP expression. Cancer Lett. 2022;531:1–13.
- Dong HL, Zeng LL, Chen WW, Zhang Q, Wang F, Wu Y, et al. N6-methyladenine-mediated aberrant activation of the IncRNA SOX2OT-GL11 loop promotes non-small-cell lung cancer stemness. Cell Death Discov. 2023;9(1):149.
- Chen WW, Wang F, Yu XY, Qi JJ, Dong HL, Cui BJ, et al. LncRNA MIR31HG fosters stemness malignant features of nonsmall cell lung cancer via H3K4me1- and H3K27Ace-mediated GLI2 expression. Oncogene. 2024;43(18):1328–40.
- 19. Khan P, Siddiqui JA, Lakshmanan I, Ganti AK, Salgia R, Jain M, et al. RNA-based therapies: a cog in the wheel of lung cancer defense. Mol Cancer. 2021;20(1):54.
- 20. Parma B, Wurdak H, Ceppi P. Harnessing mitochondrial metabolism and drug resistance in non-small cell lung cancer and beyond by blocking heat-shock proteins. Drug Resist Updat. 2022;65:100888.
- 21. Vostakolaei MA, Hatami-Baroogh L, Babaei G, Molavi O, Kordi S, Abdolalizadeh J. Hsp70 in cancer: a double agent in the battle between survival and death. J Cell Physiol. 2021;236(5):3420–44.
- 22. Rindler K, Jonak C, Alkon N, Thaler FM, Kurz H, Shaw LE, et al. Single-cell RNA sequencing reveals markers of disease progression in primary cutaneous T-cell lymphoma. Mol Cancer. 2021;20(1):124.
- Oron M, Grochowski M, Jaiswar A, Legierska J, Jastrzebski K, Nowak-Niezgoda M, et al. The molecular network of the proteasome machinery inhibition response is orchestrated by HSP70, revealing vulnerabilities in cancer cells. Cell Rep. 2022;40(13):111428.
- 24. Zhao NN, Zhang JJ, Zhao LL, Fu XN, Zhao Q, Chao M, et al. Long noncoding RNA NONHSAT079852.2 contributes to GBM recurrence by functioning as a ceRNA for has-mir-10401-3p to facilitate HSPA1A upregulation. Front Oncol. 2021;11:636632.
- 25. Jiang Y, Xu YJ, Zheng C, Ye L, Jiang P, Malik S, et al. Acetyltransferase from *Akkermansia muciniphila* blunts colorectal tumourigenesis by reprogramming tumour microenvironment. Gut. 2023;72(7):1308–18.
- Li JN, Zhu LP, Kwok HF. Nanotechnology-based approaches overcome lung cancer drug resistance through diagnosis and treatment. Drug Resist Updat. 2023:66:100904.
- 27. Cheng G, Liu D, Liang HG, Yang HM, Chen K, Zhang XP. A cluster of long non-coding RNAs exhibit diagnostic and prognostic values in renal cell carcinoma. Aging. 2019;11(21):9597–615.
- 28. Tracy KM, Tye CE, Page NA, Fritz AJ, Stein JL, Lian JB, et al. Selective expression of long non-coding RNAs in a breast cancer cell progression model. J Cell Physiol. 2018;233(2):1291–9.
- 29. Cen XN, Huang YM, Lu ZN, Shao WJ, Zhuo CY, Bao CC, et al. LncRNA IGFL2-AS1 promotes the proliferation, migration, and invasion of colon cancer cells and is associated with patient prognosis. Cancer Manag Res. 2021;13:5957–68.
- 30. Bispo S, Farias TDJ, de Araujo-Souza PS, Cintra R, Dos Santos HG, Jorge NAN, et al. Dysregulation of transcription factor networks unveils different pathways in human papillomavirus 16-positive squamous cell carcinoma and adenocarcinoma of the uterine cervix. Front Oncol. 2021;11:626187.
- 31. Qin M, Liu Q, Yang W, Wang Q, Xiang Z. IGFL2-AS1-induced suppression of HIF-1alpha degradation promotes cell proliferation and invasion in colorectal cancer by upregulating CA9. Cancer Med. 2023;12(7):8415–32.
- 32. Liu S, Wang XJ, Zhang J, Liu YB, Li BH. LncRNA IGFL2-AS1 as a cerna promotes HCT116 cell malignant proliferation via the miR-433-3p/PAK4 axis. Turk J Gastroenterol. 2023;34(5):497–507.
- 33. Zhao RM, Wang SY, Tan L, Li HJ, Liu JS, Zhang SQ. IGFL2-AS1 facilitates tongue squamous cell carcinoma progression via Wnt/beta-catenin signaling pathway. Oral Dis. 2023;29(2):469–82.
- 34. Ma Y, Liu Y, Pu YS, Cui ML, Mao ZJ, Li ZZ, et al. LncRNA IGFL2-AS1 functions as a cerna in regulating ARPP19 through competitive binding to miR-802 in gastric cancer. Mol Carcinog. 2020;59(3):311–22.
- 35. Wang H, Shi Y, Chen CH, Wen Y, Zhou Z, Yang C, et al. KLF5-induced lncRNA IGFL2-AS1 promotes basal-like breast cancer cell growth and survival by upregulating the expression of IGFL1. Cancer Lett. 2021;515:49–62.
- 36. Lee J, Kim DY, Kim Y, Shin US, Kim KS, Kim EJ. IGFL2-AS1, a long non-coding RNA, is associated with radioresistance in colorectal cancer. Int J Mol Sci. 2023;24(2):978.
- 37. Cheng B, Xie MY, Zhou Y, Li T, Liu WT, Yu WJ, et al. Vascular mimicry induced by m(6)A mediated IGFL2-AS1/AR axis contributes to pazopanib resistance in clear cell renal cell carcinoma. Cell Death Discov. 2023;9(1):121.

- 38. Pan YH, Lu XX, Shu GN, Cen JJ, Lu J, Zhou M, et al. Extracellular vesicle-mediated transfer of LncRNA IGFL2-AS1 confers sunitinib resistance in renal cell carcinoma. Cancer Res. 2023;83(1):103–16.
- 39. Lu XX, Xu QL, Tong YN, Zhang ZJ, Dun GD, Feng YY, et al. Long non-coding RNA EVADR induced by *Fusobacterium nucleatum* infection promotes colorectal cancer metastasis. Cell Rep. 2022;40(3):111127.
- 40. Wang Y, Feng YC, Gan Y, Teng L, Wang L, La T, et al. LncRNA MILIP links YBX1 to translational activation of Snai1 and promotes metastasis in clear cell renal cell carcinoma. J Exp Clin Cancer Res. 2022;41(1):260.
- 41. Wang YQ, Wei JY, Feng LY, Li OW, Huang L, Zhou SX, et al. Aberrant m5C hypermethylation mediates intrinsic resistance to gefitinib through NSUN2/YBX1/QSOX1 axis in EGFR-mutant non-small-cell lung cancer. Mol Cancer. 2023;22(1):81.
- 42. Lu ML, Zeng YY, Yu ZQ, Chen SZ, Xie JJ, Rao BQ, et al. EIF4a3-regulated circRABL2B regulates cell stemness and drug sensitivity of lung cancer via YBX1-dependent downregulation of MUC5AC expression. Int J Biol Sci. 2023;19(9):2725–39.
- 43. Lv JD, Liu YY, Mo SQ, Zhou YB, Chen FY, Cheng FR, et al. Gasdermin E mediates resistance of pancreatic adenocarcinoma to enzymatic digestion through a YBX1-mucin pathway. Nat Cell Biol. 2022;24(3):364–72.
- 44. Xie Q, Zhao S, Liu W, Cui Y, Li F, Li Z, et al. YBX1 enhances metastasis and stemness by transcriptionally regulating MUC1 in lung adenocarcinoma. Front Oncol. 2021;11:702491.
- 45. Su H, Fan G, Huang J, Qiu X. YBX1 regulated by Runx3-miR-148a-3p axis facilitates non-small-cell lung cancer progression. Cell Signal. 2021;85:110049.
- 46. Su HB, Fan GZ, Huang J, Qiu XS. LncRNA HOXC-AS3 promotes non-small-cell lung cancer growth and metastasis through upregulation of YBX1. Cell Death Dis. 2022;13(4):307.
- 47. Kumar S, Stokes J 3rd, Singh UP, Scissum Gunn K, Acharya A, Manne U, et al. Targeting Hsp70: A possible therapy for cancer. Cancer Lett. 2016;374(1):156–66.
- 48. Tang TL, Yang C, Brown HE, Huang J. Circulating heat shock protein 70 is a novel biomarker for early diagnosis of lung cancer. Dis Markers. 2018;2018:1–8.
- 49. Wang X, Wang YT, Fang ZY, Wang H, Zhang J, Zhang LF, et al. Targeting HSPA1A in ARID2-deficient lung adenocarcinoma. Natl Sci Rev. 2021;8(10):nwab014.
- 50. Kan J, Fu BQ, Zhou RS, Zhou DH, Huang YF, Zhao HW, et al. He-chan pian inhibits the metastasis of non-small cell lung cancer via the miR-205-5p-mediated regulation of the GREM1/Rap1 signaling pathway. Phytomedicine. 2022:94:153821.
- 51. Xiao L, Lan XY, Shi XP, Zhao K, Wang DR, Wang XJ, et al. Cytoplasmic RAP1 mediates cisplatin resistance of non-small cell lung cancer. Cell Death Dis. 2017;8(5):e2803-e.
- 52. Nazari M, Babakhanzadeh E, Mollazadeh A, Ahmadzade M, Mohammadi Soleimani E, Hajimaqsoudi E. HOTAIR in cancer: diagnostic, prognostic, and therapeutic perspectives. Cancer Cell Int. 2024;24(1):415.
- 53. Xu DX, Wang WH, Wang D, Ding J, Zhou YN, Zhang WB. Long noncoding RNA MALAT-1: a versatile regulator in cancer progression, metastasis, immunity, and therapeutic resistance. Non-coding RNA Res. 2024;9(2):388–406.
- 54. Zhang L, Zhao FQ, Li WF, Song GB, Kasim V, Wu SR. The biological roles and molecular mechanisms of long non-coding RNA MEG3 in the hallmarks of cancer. Cancers (Basel). 2022;14(24):6032.

Publisher's Note

Springer Nature remains neutral with regard to jurisdictional claims in published maps and institutional affiliations.